© 2019. Published by The Company of Biologists Ltd | Development (2019) 146, dev173674. doi:10.1242/dev.173674

RESEARCH REPORT

Disruption of the pancreatic vasculature in zebrafish affects islet architecture and function

Sri Teja Mullapudi, Giulia L. M. Boezio, Andrea Rossi*, Michele Marass, Ryota L. Matsuoka‡, Hiroki Matsuda§, Christian S. M. Helker¶, Yu Hsuan Carol Yang and Didier Y. R. Stainier**

ABSTRACT

A dense local vascular network is crucial for pancreatic endocrine cells to sense metabolites and secrete hormones, and understanding the interactions between the vasculature and the islets may allow for therapeutic modulation in disease conditions. Using live imaging in two models of vascular disruption in zebrafish, we identified two distinct roles for the pancreatic vasculature. At larval stages, expression of a dominant negative version of Vegfaa (dnVegfaa) in β-cells led to vascular and endocrine cell disruption with a minor impairment in β-cell function. In contrast, expression of a soluble isoform of Vegf receptor 1 (sFlt1) in β-cells blocked the formation of the pancreatic vasculature and drastically stunted glucose response, although islet architecture was not affected. Notably, these effects of dnVegfaa or sFlt1 were not observed in animals lacking *vegfaa*, *vegfab*, *kdrl*, *kdr* or *flt1* function, indicating that they interfere with multiple ligands and/or receptors. In adults, disrupted islet architecture persisted in dnVegfaa-expressing animals, whereas sFlt1-expressing animals displayed large sheets of β-cells along their pancreatic ducts, accompanied by impaired glucose tolerance in both models. Thus, our study reveals novel roles for the vasculature in patterning and function of the islet.

KEY WORDS: Pancreas, Vasculature, Beta cells, VEGF, Zebrafish

INTRODUCTION

Specialized to sense and rapidly respond to circulating metabolites, pancreatic islets are crucial in regulating glucose homeostasis. Attesting to their importance, these endocrine cell clusters are densely vascularized (Bonner-Weir, 1988), drawing up to 20 times more blood compared with the surrounding exocrine tissue (Lifson et al., 1985). Thus, understandably, when their vascular connections are severed during isolation for transplantation purposes, the islets experience ischemia, resulting in poor engraftment and survival (Pepper et al., 2013). Transplanted islets seldom achieve the high degree of vascularization observed in native pancreatic islets (Mattsson et al., 2002). Thus, elucidating the interactions between pancreatic endocrine cells and blood vessels, and exploring the consequences of their modulation, could facilitate improved designs for transplantation protocols.

During mammalian development, pancreatic progenitor cell differentiation and self-renewal, as well as expression of endocrine markers, depend on signals from the endothelium (Lammert et al., 2001; Yoshitomi and Zaret, 2004; Edsbagge et al., 2005; Magenheim et al., 2011). The vasculature also regulates β-cell function and proliferation through the establishment of a complex basement membrane (Nikolova et al., 2006; Parnaud et al., 2009). More recently, insulin secretion in β-cells was shown to be targeted towards the vasculature, owing to a basolateral vascular face in β-cells (Gan et al., 2017, 2018). Recent attempts at uncovering the role of the vasculature in mature islets using temporal inactivation of VEGFA (Reinert et al., 2013) or transgenic overexpression of a soluble isoform of VEGF receptor 1 (sFLT1) (D'Hoker et al., 2013) report that a marked decrease of pancreatic vasculature resulted in no major defects. These models achieved a reduction in islet vascular density down to 30% of wild-type levels, leading to mild hypoxia. However, it is unclear whether compensatory effects of β-cell function (Chen et al., 2017) from the spared, i.e. vascularized, islets might explain the observations made in these studies. Hence, the consequences of complete vascular depletion in an islet remain to be determined.

Owing to its many advantages (Ober et al., 2003; Beis and Stainier, 2006), the zebrafish is an ideal model to study pancreas development and function, including hepatopancreatic duct development (Manfroid et al., 2012; Villasenor and Stainier, 2017), β-cell development (Ninov et al., 2012; Matsuda et al., 2013), α-to-β-cell transdifferentiation (Ye et al., 2015; Lu et al., 2016), β-cell regeneration (Andersson et al., 2012; Delaspre et al., 2015), islet innervation (Yang et al., 2018) and vascularization (Hen et al., 2015; Toselli et al., 2019), as well as endocrine cell motility (Freudenblum et al., 2018). The developing zebrafish has a single functional primary islet (Biemar et al., 2001; Field et al., 2003), thereby facilitating the observation of all the organism's β-cells and their interactions with blood vessels. In this study, combining live imaging with two potent tools to disrupt the pancreatic vasculature – a dominant negative form of Vegfaa (dnVegfaa) and sFlt1 – we identified distinct roles for the pancreatic vasculature in regulating islet architecture and function.

RESULTS AND DISCUSSION

β-Cell-specific dnVegfaa expression disrupts pancreatic islet architecture

In the developing zebrafish pancreas, *pdx1*-positive progenitors appear at around the 10-somite stage [13.25 h post fertilization (hpf)] and preproinsulin (*ins*)-positive cells around the 12-somite stage (14 hpf), followed by their migration to the midline to form the endocrine islet (24 hpf) (Biemar et al., 2001; Field et al., 2003). At this stage, the embryonic islet is sandwiched between the dorsal

Department of Developmental Genetics, Max Planck Institute for Heart and Lung Research, 61231 Bad Nauheim, Germany.
*Present address: Leibniz Institute IUF, Model Development Unit, 40225 Düsseldorf, Germany. ‡Present address: Department of Cardiovascular and Metabolic Sciences, Lerner Research Institute, Cleveland Clinic, Cleveland, OH 44106, USA. §Present address: Department of Biomedical Sciences, College of Life Sciences, Ritsumeikan University, Kusatsu 525-8577, Japan. ¶Present address: Philipps-University Marburg, Faculty of Biology, Cell Signaling and Dynamics, 35043 Marburg, Germany.

**Author for correspondence (didier.stainier@mpi-bn.mpg.de)

D.Y.R.S., 0000-0002-0382-0026

Received 13 November 2018; Accepted 3 October 2019

Development (2019) 146, dev173674. doi:10.1242/dev.173674

aorta (DA) and the posterior cardinal vein (PCV). Subsequently, between 36 and 72 hpf, endothelial cells from the subintestinal vein (SIV) and the anterior PCV (aPCV) invade the islet to form the pancreatic vasculature (Hen et al., 2015). To interrupt vascularization of the islet, we expressed dnVegfaa under the control of the *ins* promoter. dnVegfaa, with its inability to bind VEGF receptors, although retaining its property to dimerize with multiple Vegf family members, possesses potent anti-angiogenic activity (Rossi et al., 2016).

We did not observe any defects in early embryonic islet formation or vascular development in 28 hpf embryos upon dnVegfaa expression (Fig. 1A,B). However, by 48 hpf, the endocrine islet was completely dispersed (Fig. 1C,D), and it remained disrupted at later stages, despite the fact that β-cells maintained contact with other endocrine cells (Fig. S1A,B), including α-cells (Fig. S1C,D). No significant change in β-cell number was observed (Fig. S1E). *In vivo* time-lapse imaging revealed that, although the β-cells in *Tg(ins:Tomato)* embryos migrated together towards the aPCV, the β-cells in *Tg(ins:Tomato-P2A-dnvegfaa)* embryos began separating between 38 and 42 hpf (Fig. 1E,F, Movies 1 and 2). We also observed defects in some intersegmental vessels (ISVs) at 34 hpf (Fig. 1F). Interestingly, the dnVegfaa-expressing β-cells were still closely associated with endothelial cells, and only the ISVs situated directly above the dnVegfaa-expressing β-cells exhibited defects (Fig. 1F-F′′′′). A possible explanation for this islet dispersion is that interference with Vegf signaling affects the expression of endothelial cell-derived factors (Johansson et al., 2006) and extracellular matrix deposition in the islet (Nikolova et al., 2007), resulting in altered migratory signals to the β-cells (Peiris et al., 2014; Hogan and Hull, 2017). Together, these observations indicate a rather short-ranged anti-angiogenic effect of dnVegfaa, resulting in the local disruption of the vasculature, itself leading to islet dispersion.

β-Cell-specific dnVegfaa expression interferes with multiple ligands and/or receptors

To gain mechanistic insight into how dnVegfaa-mediated vascular disruption causes endocrine cell dispersal, we wanted to determine the likelihood that an isolated β-cell expressing dnVegfaa would disperse away from the islet and whether Vegf signaling pathway mutants also exhibited these phenotypes. First, the *Tg(ins:Tomato-2A-dnVegfaa)* construct was injected into *Tg(ins:GFP)* embryos to overexpress dnVegfaa in a subset of β-cells. The islet remained intact in these mosaic animals when dnVegfaa was expressed in 1-20% of the β-cells (Fig. 2A,B). When 20-50% of the β-cells expressed dnVegfaa, a few β-cells, not necessarily the dnVegfaa-expressing ones, were observed away from the islet cluster (Fig. 2A). Severe dispersion of β-cells was only observed when more than half of the β-cells expressed dnVegfaa (Fig. 2B). Together, these observations indicate an indirect and dose-dependent role for dnVegfaa in the dispersal of β-cells.

Disruption of islet architecture occurred even when dnVegfaa expression was induced postembryonically (Fig. S1F-H), suggesting that dnVegfaa was not merely interfering with early endocrine cell migration, but rather affected an active mechanism regulating islet architecture. To gain further insights into this

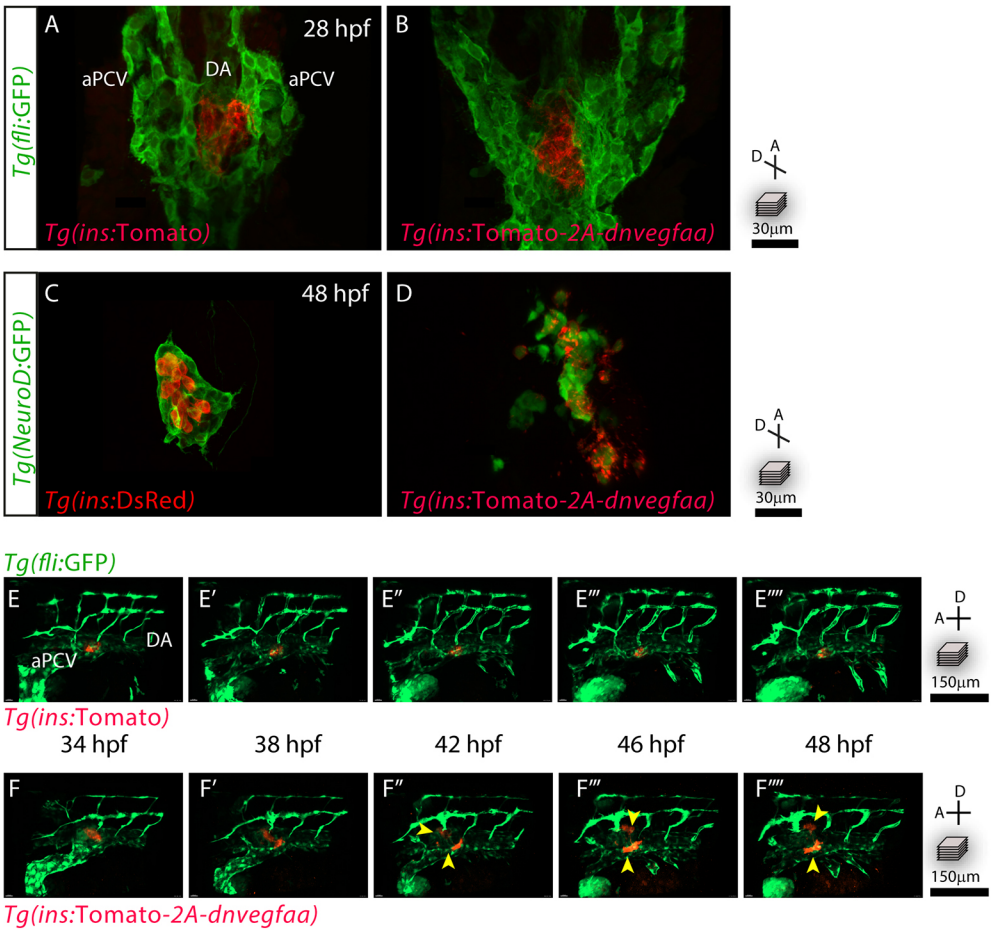

Fig. 1. β-Cell-specific dnVegfaa expression disrupts pancreatic islet architecture. (A,B) Pancreatic β-cells (red) and the endothelial cells (green) in 28 hpf *Tg(ins:Tomato); Tg(fli:GFP)* and *Tg(fli:GFP); Tg(ins:dnvegfaa)* embryos, viewed ventrally. (C,D) Pancreatic endocrine cells (green) and β-cells (red) in 48 hpf *Tg(NeuroD:GFP); Tg(ins:DsRed)* and *Tg(NeuroD:GFP); Tg(ins:dnvegfaa)* embryos, viewed ventrally. (E-F) Confocal projection images of *Tg(ins:Tomato); Tg(fli:GFP)* and *Tg(ins:dnvegfaa); Tg(fli:GFP)* embryos from 34 to 48 hpf, viewed laterally. Yellow arrowheads point to dispersing β-cells. Maximum intensity projections are presented. A, anterior; D, dorsal.

Development (2019) 146, dev173674. doi:10.1242/dev.173674

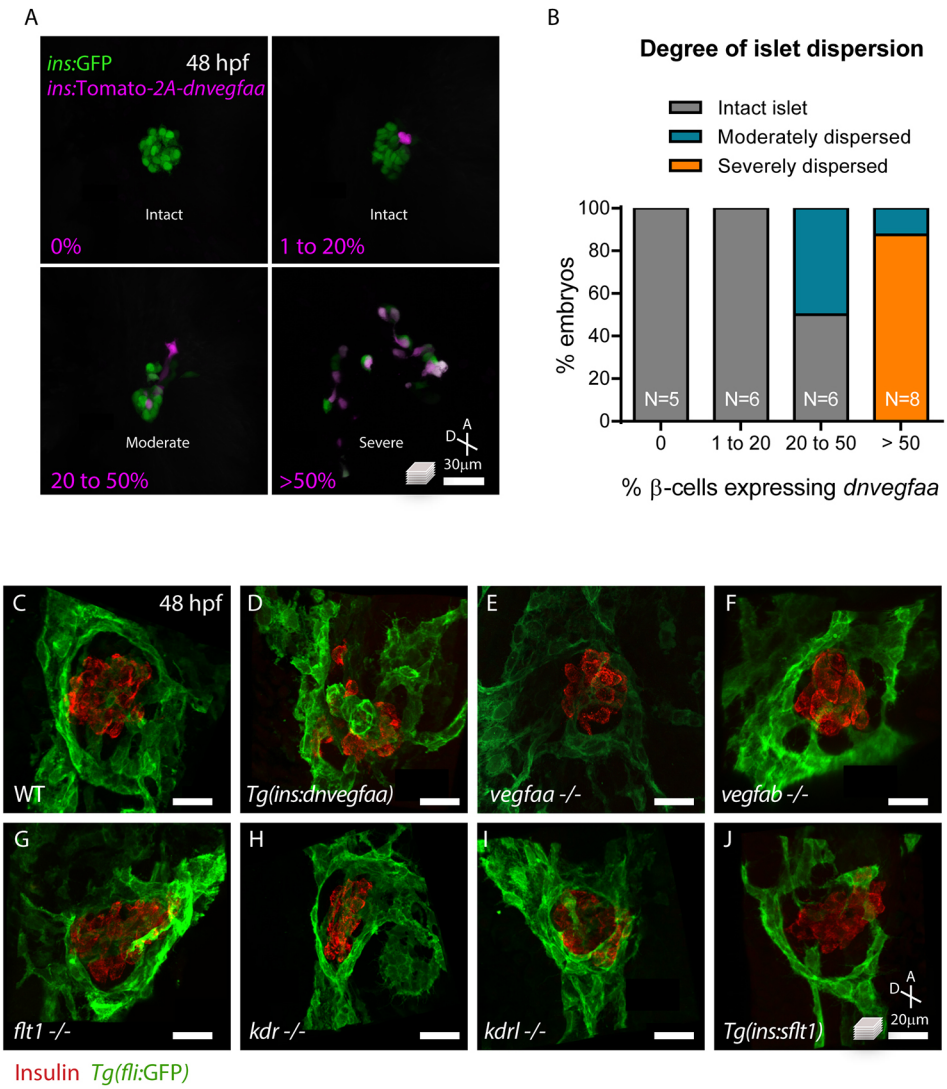

Fig. 2. dnVegfaa exerts a dose-dependent effect on β-cell dispersion. (A) β-Cells (green) from 48 hpf *Tg(ins:GFP)* embryos with mosaic *Tg(ins:dnvegfaa)* expression. The percentage of β-cells expressing *dnvegfaa* (magenta) is indicated, as is the severity of islet dispersion (intact, moderate or severe; white). (B) Quantification of embryos displaying varying severity of islet dispersion. (C-J) Immunostaining for insulin (β-cells, red) and endothelial cells (green) in 48 hpf *Tg(fli:GFP)* embryos, in combination with the indicated transgenic or mutant line, *n*=3-5 animals per genotype. Maximum intensity projections are presented.
A, anterior; D, dorsal.

mechanism, we examined the expression of several reporter lines in the developing islet at 48 hpf. We detected *vegfaa* promoter activity in β-cells, as well as in nearby non-endocrine cells, and *vegfab* promoter activity in endocrine cells (Fig. S2A-C). Promoter activity of receptor genes implicated in Vegf and Pdgf signaling, such as *kdrl*, *pdgfrb* and *flt1*, was also observed in the vessels within the islet (Fig. S2D,E). Next, we analyzed zebrafish mutants for Vegf ligand and receptor genes including *vegfaa*, *vegfab*, *flt1*, *kdr* and *kdrl*, and compared their β-cell architecture and surrounding vasculature with those in *Tg(ins:dnvegfaa)* embryos. In 48 hpf wild-type embryos, the β-cells clustered tightly together, with blood vessels running along the periphery of the islet and three to four intra-islet vessels (Fig. 2C, Movie 3). In *Tg(ins:dnvegfaa)* embryos, the β-cells were dispersed, and the surrounding and intra-islet vasculature was also disrupted. Notably, the β-cells were still in contact with blood vessels (Fig. 2D and Fig. S3A,B). However, unlike wild-type β-cells, which have multiple contact points with the vasculature, dnVegfaa-expressing β-cells contacted the vasculature at only one point (Fig. 2C,D). In all the mutants examined, we did not detect major defects in β-cell clustering or peripheral/intra-islet vascularization (Fig. 2E-I). Notably, the *Tg(ins:sflt1)* line, which was generated as an additional dominant negative approach to interfere with the vasculature near the β-cells, contained islets with an intact β-cell architecture but no intra-islet vasculature (Fig. 2J, Movie 4). These observations, combined with the effects of dnVegfaa on the β-cell vasculature, suggest that during the establishment and maintenance of islet vascularization there is redundancy amongst the Vegf receptor genes in zebrafish (Rossi et al., 2016; Toselli et al., 2019); in mouse however, *Kdr* mutants exhibit severe vascular defects (Shalaby et al., 1995). In addition, because the expression levels of the Vegf receptor genes in β-cells are minimal (Table S1) (Tarifeño-Saldivia et al., 2017; Salem et al., 2019), we postulate that dnVegfaa and sFlt1 do not affect β-cells directly.

The mechanistic differences between dnVegfaa and sFlt1 action are not yet completely understood. sFlt1 can attenuate Vegfa- and Vegfb-mediated signaling without affecting Vegfc- or Vegfd-dependent signaling (Kendall and Thomas, 1993; Koch and Claesson-Welsh, 2012). In contrast, dnVegfaa can potentially dimerize with all Vegf ligands, sterically hinder Vegfr2 activation by other ligands and thereby block all Vegfr2-mediated signaling, including Vegfc- and Vegfd-dependent processes (Rossi et al., 2016). In addition, steric inhibition of Vegfr2 by dnVegfaa might also block the angiogenic action of other ligands such as gremlin (Mitola et al., 2010). Thus, it is possible that residual Vegf receptor signaling in *Tg(ins:sFlt1)* animals is responsible for the differences

Development (2019) 146, dev173674. doi:10.1242/dev.173674

in the vascular phenotypes between the models. Further experiments expressing dnVegfaa in other vascular beds and studying endothelial cell behavior at single-cell resolution are needed to improve our mechanistic understanding of these reagents.

β-Cell-specific sFlt1 expression results in impaired β-cell function due to the lack of pancreatic vasculature

Functional β-cells are crucial in regulating glucose levels at early embryonic stages in zebrafish (Jurczyk et al., 2011). Activity of the key gluconeogenic gene, *pck1*, results in increasing glucose levels in larvae, which peaks at ∼120 hpf (Gut et al., 2013). To determine the effects of dispersed or non-vascularized islets on β-cells, we analyzed the pancreatic vasculature and β-cell function in 120 hpf animals. The pancreas in wild-type animals is densely vascularized with an SIV-derived vessel running along the pancreatic duct, as well as multiple blood vessels within the islet, as previously reported (Hen et al., 2015) (Fig. 3A-A″). Using live imaging in *Tg(gata1:DsRed); Tg(fli:GFP)* animals, active blood circulation was observed within these islets at 120 hpf (Movie 5). Similar to observations at 48 hpf, dispersion of the β-cells was still observed in 120 hpf *Tg(ins:Tomato-2A-dnvegfaa)* animals. These β-cells remained in close proximity to blood vessels (Fig. 3B-B″ and Fig. S3A,B), and blood circulation was also observed in these pancreata (Movie 6). In contrast, the pancreas in 120 hpf *Tg(ins:sflt1)* animals was entirely devoid of blood vessels (Fig. 3C-C″), resulting in a lack of β-cell-vascular interactions. This observation was also supported by the absence of any detectable blood circulation in the islets of *Tg(ins:sflt1)* animals (Movie 7).

Although glucose-stimulated insulin secretion assays have been performed *in vitro* to assess β-cell function in models of vascular disruption (D'Hoker et al., 2013; Reinert et al., 2013), these experiments could be limited by confounding hypoxic effects in the isolated islets, even from control animals. In contrast, our models offer the advantage of being able to visualize responses to glucose *in vivo*. To this aim, we used calcium imaging in β-cells to determine their responsiveness to glucose. β-Cells in 120 hpf *Tg(ins:GCaMP5)* animals were imaged with or without exogenous glucose and scored as being responsive, depending on visual changes in fluorescence

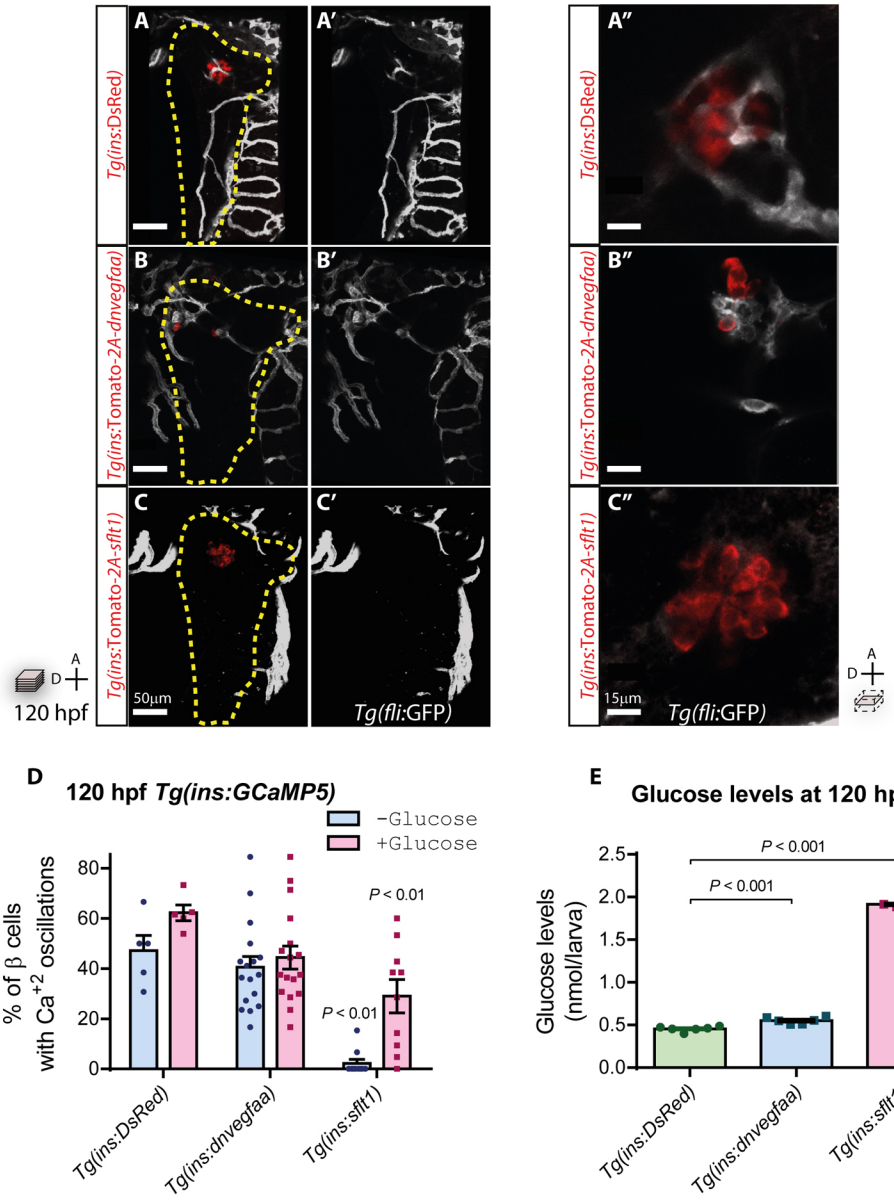

Fig. 3. sFlt1 expression in β-cells severely impairs their function. (A-C) Confocal projection images of the vasculature (white) in 120 hpf *Tg(fli:GFP)* larvae, in combination with the indicated transgenic line. Yellow dashed lines outline the pancreas. A′-C′ show the endothelial cells. (A″-C″) Confocal planes of β-cells (red) and the surrounding vasculature (white) in 120 hpf *Tg(fli:GFP)* larvae, in combination with the indicated transgenic line. (D) Percentage of β-cells responsive to physiological (−Glucose) and exogenous (+Glucose) glucose, measured as visual fluctuations in fluorescence in 120 hpf *Tg(ins:GCaMP5)* larvae, *n*=5-17 animals. (E) Glucose levels in 120 hpf animals, *n*=4-6 replicates, 10 animals per replicate. Data are mean±s.e.m; individual data points are shown. *P*-values from *t*-tests are presented. A, anterior; D, dorsal.

Development (2019) 146, dev173674. doi:10.1242/dev.173674

intensity (Fig. S4A-G). In *Tg(ins:DsRed)* animals, 47±12% (mean±s.e.m) of the β-cells responded to endogenous glucose and 62±6% to exogenous glucose (Fig. 3D). In *Tg(ins:dnvegfaa)* animals, 40±17% of the β-cells responded to endogenous glucose and 44±18% of them to exogenous glucose. In contrast, in *Tg(ins:sflt1)* animals, only 2 (+4 or −2)% of the β-cells responded to endogenous glucose, likely owing to the lack of vasculature and blood flow within the islet. Addition of exogenous glucose, which leads to a higher concentration throughout the animal (including by its non-vascularized β-cells), resulted in a much higher fraction of glucose-responsive β-cells (29±19%), suggesting that they retain their ability to respond to glucose. Furthermore, free glucose levels, which serve as a measure of functional β-cell mass, were threefold higher in *Tg(ins:sflt1)* animals, but only 20% higher in *Tg(ins:dnvegfaa)* animals (Fig. 3E). *pdx1* mRNA levels in 120 hpf *Tg(ins:sflt1)* animals were similar to those in *Tg(ins:dsRed)* animals (Fig. S4H), suggesting that differences in β-cell differentiation are unlikely, whereas higher *ins* mRNA expression levels (Fig. S4I) could be a compensatory response to elevated glucose levels. Together, these observations indicate that although β-cells in *Tg(ins:sflt1)* animals are capable of responding to glucose, the lack of pancreatic vasculature severely limits their function.

β-Cell-specific expression of dnVegfaa or sFlt1 influences islet architecture and function in adult stages

Using a combination of imaging and blood glucose readouts, we next aimed to examine whether the effects of β-cell-specific expression of dnVegfaa or sFlt1 persisted into adulthood, and how they affected glucose homeostasis. Wild-type and *Tg(ins:DsRed)* zebrafish contain a primary islet in the anterior head of their pancreas, along with several smaller secondary islets located along their pancreatic ducts (Fig. 4A) (Chen et al., 2007). The primary islet is densely vascularized, and large numbers of β-cells are clustered at the core, with almost every β-cell in direct contact with blood vessels (Fig. 4B and Fig. S5A).

β-Cells in *Tg(ins:dnVegfaa)* animals were dispersed throughout the pancreas with no clear indication of a primary islet (Fig. 4C), although a greater density of β-cells was observed in the head of the pancreas (Fig. 4C). A small fraction of the dispersed β-cells remained in contact with endothelial cells (Fig. 4D). In 72 hpf animals, we observed a few β-cells in the blood circulation (Movie 8). To assess whether these circulating β-cells were functional, and to quantify pancreatic *ins* expression, we isolated RNA from several sections of adult fish and measured *ins* mRNA levels (Fig. S5E). Compared with wild-type samples, lower levels of *ins* mRNA were detected in sections containing the anterior pancreas (containing the primary islet) and the posterior pancreas (containing secondary islets) of *Tg(ins:dnvegfaa)* animals (Fig. S5F), supporting our imaging observations of a decrease in total β-cell volume (Fig. S5G) and volume of β-cells in secondary islets (Fig. S5H). No significant increase in *ins* mRNA levels was detected in the head or tail sections of *Tg(ins:dnvegfaa)* animals compared with wild type (Fig. S5F), making it unlikely that the circulating β-cells were functional. The lack of large secondary islets (Fig. S5H) indicates that the β-cells are unable to form clusters in these animals, in line with observations at larval stages (Fig. 3B).

Although *Tg(ins:sflt1)* animals contained a prominent primary islet and several secondary islets along the pancreatic ducts, the morphology of these islets appeared to be drastically altered (Fig. 4E). Strikingly, the β-cells in the primary islet appeared as a spherical shell, giving rise to a 'hollow' core (Fig. 4F), and amounted to a lower overall β-cell volume (Fig. S5G). No blood vessels were detected in the core of the islet, or in close proximity to the β-cells, although DAPI-positive cells were observed in the core (Fig. S5D). β-Cell clusters in secondary islets in these animals also exhibited an elongated sheet-like morphology, enveloping the pancreatic ducts, with β-cell volume in most islets comparable with that seen in wild types (Fig. S5C,H). This arrangement was in stark contrast to the spherical secondary islets observed in *Tg(ins:Tomato)* animals (Fig. S5A). The lack of vasculature and the single-layered arrangement indicate an adaptation of the β-cells to a possibly hypoxic environment within the islet owing to sFlt1 expression. Our model likely achieves a higher degree of vascular depletion compared with the mouse sFLT1 expression model (D'Hoker et al., 2013), possibly explaining the morphological differences observed.

As a measure of functional β-cell mass, we determined fasting blood glucose levels and found that, compared with *Tg(ins:Tomato)* controls, *Tg(ins:sflt1)* animals did not exhibit any major differences, whereas *Tg(ins:dnvegfaa)* animals displayed mildly lower levels (Fig. 4G). However, a glucose tolerance test in these animals revealed an impaired ability to clear glucose in both *Tg(ins:dnvegfaa)* and *Tg(ins:sflt1)* animals compared with *Tg(ins:Tomato)* controls (Fig. 4H). The dispersed islet architecture in *Tg(ins:dnvegfaa)* animals likely affects the interactions between β-cells, and could thereby alter their coupling, which is crucial to mount a synchronized response to glucose (Ravier et al., 2005). Likewise, the lack of islet vasculature in *Tg(ins:sflt1)* animals could be responsible for the reduced ability of their β-cells to sense circulating glucose, as well as for a reduced ability for secreted insulin to reach the blood circulation (D'Hoker et al., 2013; Reinert et al., 2013).

In conclusion, our study combines live imaging with potent tools to disrupt the vasculature; it reveals two distinct consequences of abrogating interactions between pancreatic islets and the vasculature. Despite variation in cell layout, pancreatic endocrine cells across species cluster together as micro-organs (Steiner et al., 2010), facilitating cell-cell interactions. It will be important to investigate the molecular mechanisms that lead to endocrine cell clustering and the role of the resulting interactions on their function. In addition, it will be interesting to further investigate the morphological adaptations observed in islets with depleted vasculature. Altogether, these findings should help design improved stem cell-derived cell transplantation strategies with reduced ischemia, immunogenicity and inflammation, thereby ensuring cell and islet engraftment and long-term function.

MATERIALS AND METHODS

Zebrafish lines

Transgenic lines used in the study were: *Tg(ins:GFP)^{zf5}* (Huang et al., 2001), *Tg(gata1:DsRed)^{sd2}* (Traver et al., 2003), *Tg(fli1a:GFP)^{y1}* [referred to as *Tg(fli:GFP)*; Lawson and Weinstein, 2002], *Tg(ins:DsRed)^{m1018}* (Anderson et al., 2009), *TgBAC(neurod:EGFP)^{nl1}* (Obholzer et al., 2008), *TgBAC(vegfaa:EGFP)^{pd260}* (Karra et al., 2018), *Tg(pdgfrb:GFP)^{ncv22Tg}* (Ando et al., 2016), *Tg(kdrl:tagBFP)^{mu293}* (Matsuoka et al., 2016), *Tg(-0.8flt1:RFP)^{hu5333}* (Bussmann et al., 2010) and *Tg(UAS-E1b:NfsB-mCherry)^{c264}* (Davison et al., 2007).

Mutant lines used in the study were: *vegfaa^{bns1}* (Rossi et al., 2016), *vegfab^{bns92}* (Rossi et al., 2016), *kdrl^{hu5088}* (Hogan et al., 2009), *flt1^{bns29}* (Matsuoka et al., 2016) and *kdr^{bns32}*.

Zebrafish husbandry was performed under standard conditions in accordance with institutional (Max Planck Gesellschaft) and national ethical and animal welfare guidelines approved by the ethics committee for animal experiments at the Regierungspräsidium Darmstadt, Germany.

Generation of new transgenic and mutant lines

We used 1.1 kb of the zebrafish *ins* promoter to drive β-cell-specific expression of proteins in the following transgenic lines: *Tg(ins:TagRFP-T-P2A-sflt1)^{bns286}*

Development (2019) 146, dev173674. doi:10.1242/dev.173674

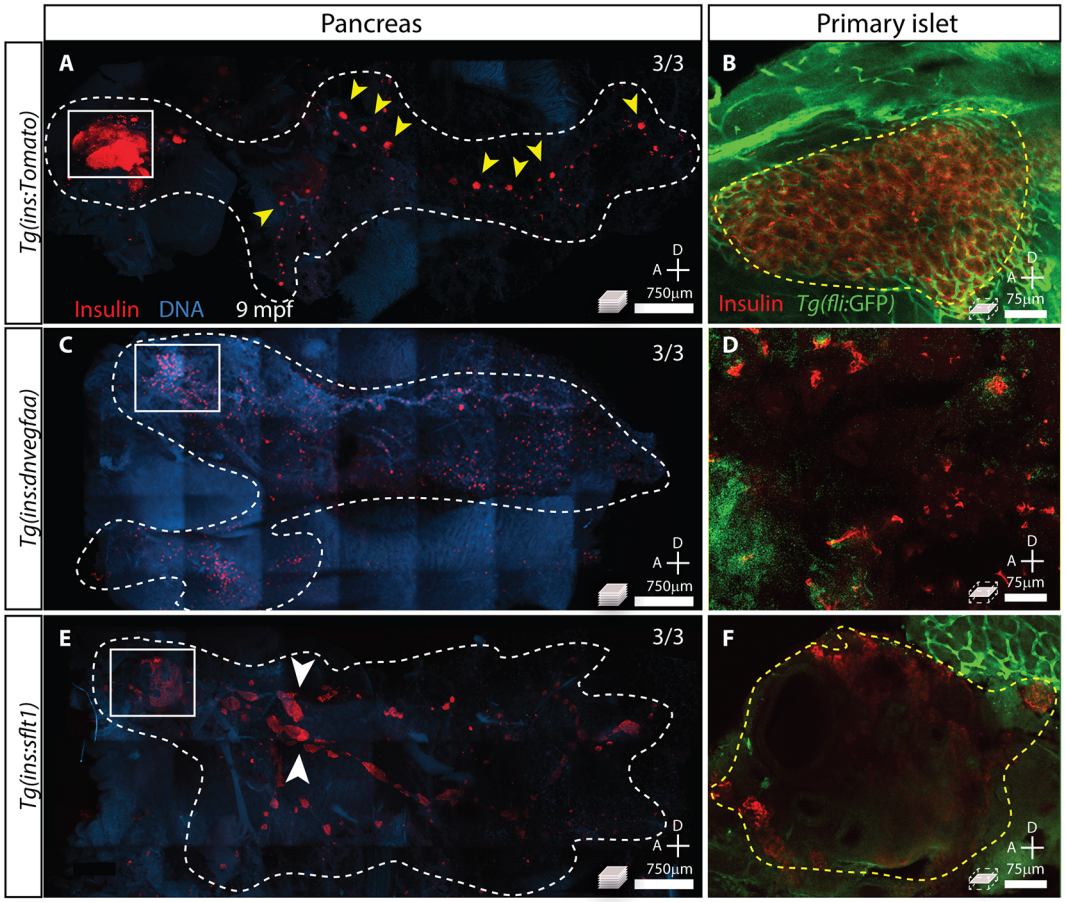

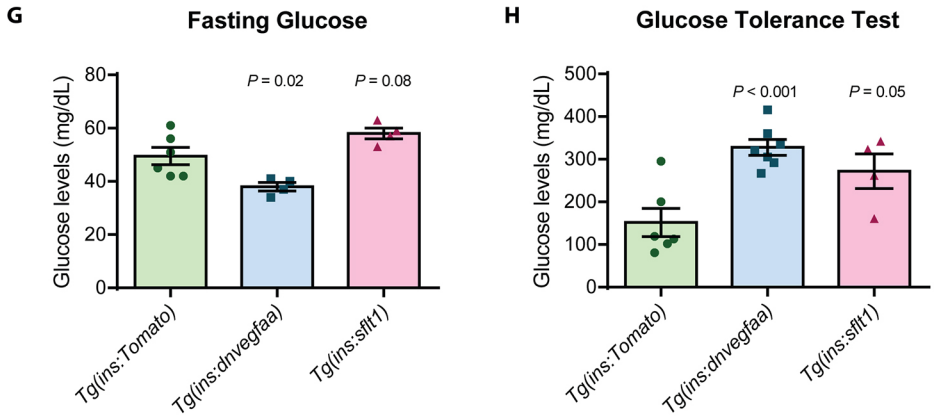

Fig. 4. β-Cell-specific expression of dnVegfaa or sFlt1 influences islet architecture and function in adult stages. (A,C,E) Whole-mount immunostaining for β-cells (insulin, red) in pancreas (white dashed outline) and intestine from 9 months postfertilization (mpf) zebrafish after CLARITY-based tissue clearing. Yellow arrowheads point to secondary islets along the pancreatic duct. White arrowheads point to sheets of β-cells along the ducts observed in *Tg(ins:sflt1)* animals. Maximum projection images are presented. (B,D,F) Whole-mount immunostaining for β-cells (insulin, red) and vasculature (green) in the primary pancreatic islet (magnification of white boxed areas in A,C and E, respectively). Images are single confocal planes. Yellow dashed line outlines the primary pancreatic islet. (G) Fasting blood glucose levels in adult zebrafish, measured after three days of fasting, *n*=4-6 animals. (H) Blood glucose levels in adult zebrafish, 90 min after intraperitoneal administration of a glucose bolus, *n*=4-7 animals. Data are mean±s.e.m.; individual data points are shown. *P*-values from *t*-tests are presented. A, anterior; D, dorsal.

[referred to as *Tg(ins:sflt1)*], *Tg(ins:TagRFP-T-P2A-dnvegfaa)*^{bns284} containing the T46A mutant isoform of Vegfaa-121 [*Tg(ins:dnvegfaa)*; Rossi et al., 2016], *Tg(ins:memTdTomato-P2A-dnvegfaa)*^{bns282} [*Tg(ins:Tomato-P2A-dnvegfaa)*], *Tg(ins:memTdTomato-P2A)*^{bns211} [*Tg(ins:Tomato)*], *Tg(ins:LoxP-Gfp-LoxP-memTom-P2A-dnvegfaa)*^{bns287} and *Tg(ins:GCaMP5)*^{bns306}. All transgenic lines were generated using I-SceI meganuclease-mediated transgenesis (Thermes et al., 2002). Multiple founders were identified and analyzed to ensure consistent expression of reporters and observed phenotypes.

To generate the *TgBAC(pdx1:CreERT)*^{bns307} line, a BAC containing 200 kb of the *pdx1* locus was used and recombineering steps were performed as described previously (Helker et al., 2019) with the inclusion of a CreERT2-Kanamycin cassette. The *TgBAC(vegfab:gal4ff)*^{bns273} line was

Development (2019) 146, dev173674. doi:10.1242/dev.173674

generated by following the standard BAC recombineering protocol described previously (Bussmann and Schulte-Merker, 2011). Briefly, the BAC clone DKEY-234H13 (Source Bioscience) was engineered to replace the *vegfab* start codon with *gal4ff*. The engineered construct was injected into one-cell stage embryos together with Tol2 transposase mRNA.

To generate mutants for *kdr*, the CRISPR design platform (http://crispr.mit.edu) was used to design sgRNAs binding to exon 6, and constructs were assembled and mutagenesis was performed as described previously (Jao et al., 2013; Varshney et al., 2015). An 8 bp deletion was obtained.

In vivo imaging

To image blood flow in 120 hpf zebrafish and circulating cells in 72 hpf zebrafish, the animals were mounted laterally in 0.8% low-melting agarose with 0.02% Tricaine. A Zeiss Spinning Disk confocal microscope was used to acquire 5 s of images at 40 frames per second from multiple planes in the islet.

For calcium imaging, *Tg(ins:GcaMP5)* larvae were treated from 72 to 120 hpf with 1.5 mM of Pck1 inhibitor 3-mercaptopicolinic acid (3-MPA) in Hepes-buffered egg water (Jurczyk et al., 2011). At 120 hpf, the larvae were mounted in 0.8% low-melting agarose with 0.02% Tricaine. An LSM880 (Zeiss) confocal microscope was used to image multiple planes in the islet for 10 min without addition of glucose, and for 15 min post glucose addition. Images were processed on Imaris (Bitplane) and maximum projection images were generated.

Whole-mount immunostaining

Immunostaining was performed as described previously (Mullapudi et al., 2018). Antibody dilutions used are as follows: guinea pig anti-insulin polyclonal (1:100, A0564, Thermo Fisher Scientific), mouse anti-Glucagon (1:300, G2654, Sigma-Aldrich), rabbit anti-tagRFP (1:200, AB233, Evrogen), chicken anti-GFP (1:300, GFP-1010, Aves), goat anti-guinea pig AlexaFluor568 (1:300, A-11075, Thermo Fisher Scientific), goat anti-chicken AlexaFluor488 (1:500, A-11039, Thermo Fisher Scientific). For CLARITY-based tissue clearing, digestive tracts of adult zebrafish were fixed and cleared according to the recommended protocol (Chung and Deisseroth, 2013) using the X-CLARITY Tissue Clearing System (Biozym GmbH). β-Cell volume was measured using the 'Surface' tool in Imaris (Bitplane). For total β-cell volume quantification, the sum of the volumes encompassed by all surfaces was computed. For quantification of secondary islet volume, all islets except the primary islet were included for analysis. The volumes of the individual islets were computed and plotted.

Glucose measurements

Glucose measurements in larvae and adults were performed as described previously (Eames et al., 2010; Jurczyk et al., 2011; Matsuda et al., 2018). The glucose tolerance test was performed by injecting a 0.1 mg/µl glucose (Sigma-Aldrich) solution intraperitoneally at 1 mg/g fish weight (Eames et al., 2010). The injected animals were incubated at 28.5°C for 90 min, and then euthanized to collect blood and perform glucose measurements using a FreeStyle Freedom Lite Glucose Meter (Abbott).

Quantitative PCR

Total RNA from sections of adult zebrafish was extracted using TRIZOL (Ambion) and then cleaned with RNA Clean & Concentrator-5 (Zymo Research). Then 500 ng RNA was used to synthesize cDNA using the Maxima First-Strand cDNA kit (Thermo Fisher Scientific). SYBR Green (Thermo Fisher Scientific) was used to quantify *ins* expression levels on a CFX connect Real-time System (Bio Rad) and normalized to *rpl13* expression across samples. Primers used for *ins* were 5′-TTTAAATGCAAAG-TCAGCCACCTCAG-3′ and 5′-TTTAAATGCAAAGTCAGCCACCTC-AG-3′; and for *pdx1* primers were 5′-GGACCAGCCAAATCTTACCG-3′ and 5′-CCTCGGCCTCGACCATATA-3′.

Acknowledgements

We thank Radhan Ramadass for help with microscopy; Rashmi Priya, Sébastien Gauvrit, Rubén Marin Juez, Anabela Bensimon Brito and Zacharias Kontarakis for comments and suggestions; and Martin Laszczyk and the rest of the animal caretaking team for zebrafish care.

Competing interests

The authors declare no competing or financial interests.

Author contributions

Conceptualization: S.T.M., A.R., Y.H.C.Y., D.Y.R.S.; Methodology: S.T.M., Y.H.C.Y.; Validation: S.T.M., G.L.M.B.; Formal analysis: S.T.M., G.L.M.B.; Investigation: S.T.M., G.L.M.B.; Resources: S.T.M., A.R., M.M., R.L.M., H.M., C.S.M.H., Y.H.C.Y., D.Y.R.S.; Writing - original draft: S.T.M., D.Y.R.S.; Writing - review & editing: S.T.M., G.L.M.B., A.R., M.M., R.L.M., H.M., Y.H.C.Y., D.Y.R.S.; Visualization: S.T.M., G.L.M.B., Y.H.C.Y.; Supervision: Y.H.C.Y., D.Y.R.S.; Project administration: S.T.M., D.Y.R.S.; Funding acquisition: C.S.M.H., D.Y.R.S.

Funding

These studies were supported by funding from the Max-Planck-Gesellschaft.

Supplementary information

Supplementary information available online at
http://dev.biologists.org/lookup/doi/10.1242/dev.173674.supplemental

References

Anderson, R. M., Bosch, J. A., Goll, M. G., Hesselson, D., Dong, P. D. S., Shin, D., Chi, N. C., Shin, C. H., Schlegel, A., Halpern, M. et al. (2009). Loss of Dnmt1 catalytic activity reveals multiple roles for DNA methylation during pancreas development and regeneration. *Dev. Biol.* **334**, 213-223. doi:10.1016/j.ydbio.2009.07.017

Andersson, O., Adams, B. A., Yoo, D., Ellis, G. C., Gut, P., Anderson, R. M., German, M. S. and Stainier, D. Y. R. (2012). Adenosine signaling promotes regeneration of pancreatic beta cells in vivo. *Cell Metab.* **15**, 885-894. doi:10.1016/j.cmet.2012.04.018

Ando, K., Fukuhara, S., Izumi, N., Nakajima, H., Fukui, H., Kelsh, R. N. and Mochizuki, N. (2016). Clarification of mural cell coverage of vascular endothelial cells by live imaging of zebrafish. *Development* **143**, 1328. doi:10.1242/dev.132654

Beis, D. and Stainier, D. Y. R. (2006). In vivo cell biology: following the zebrafish trend. *Trends Cell Biol.* **16**, 105-112. doi:10.1016/j.tcb.2005.12.001

Biemar, F., Argenton, F., Schmidtke, R., Epperlein, S., Peers, B. and Driever, W. (2001). Pancreas development in zebrafish: early dispersed appearance of endocrine hormone expressing cells and their convergence to form the definitive islet. *Dev. Biol.* **230**, 189-203. doi:10.1006/dbio.2000.0103

Bonner-Weir, S. (1988). Morphological evidence for pancreatic polarity of beta-cell within islets of Langerhans. *Diabetes* **37**, 616-621. doi:10.2337/diab.37.5.616

Bussmann, J. and Schulte-Merker, S. (2011). Rapid BAC selection for tol2-mediated transgenesis in zebrafish. *Development* **138**, 4327-4332. doi:10.1242/dev.068080

Bussmann, J., Bos, F. L., Urasaki, A., Kawakami, K., Duckers, H. J. and Schulte-Merker, S. (2010). Arteries provide essential guidance cues for lymphatic endothelial cells in the zebrafish trunk. *Development* **137**, 2653. doi:10.1242/dev.048207

Chen, S., Li, C., Yuan, G. and Xie, F. (2007). Anatomical and histological observation on the pancreas in adult zebrafish. *Pancreas* **34**, 120-125. doi:10.1097/01.mpa.0000246661.23128.8c

Chen, C., Cohrs, C. M., Stertmann, J., Bozsak, R. and Speier, S. (2017). Human beta cell mass and function in diabetes: Recent advances in knowledge and technologies to understand disease pathogenesis. *Mol. Metab.* **6**, 943-957. doi:10.1016/j.molmet.2017.06.019

Chung, K. and Deisseroth, K. (2013). CLARITY for mapping the nervous system. *Nat. Methods* **10**, 508-513. doi:10.1038/nmeth.2481

D'Hoker, J., De Leu, N., Heremans, Y., Baeyens, L., Minami, K., Ying, C., Lavens, A., Chintinne, M., Stange, G., Magenheim, J. et al. (2013). Conditional hypovascularization and hypoxia in islets do not overtly influence adult beta-cell mass or function. *Diabetes* **62**, 4165-4173. doi:10.2337/db12-1827

Davison, J. M., Akitake, C. M., Goll, M. G., Rhee, J. M., Gosse, N., Baier, H., Halpern, M. E., Leach, S. D. and Parsons, M. J. (2007). Transactivation from Gal4-VP16 transgenic insertions for tissue-specific cell labeling and ablation in zebrafish. *Dev. Biol.* **304**, 811-824. doi:10.1016/j.ydbio.2007.01.033

Delaspre, F., Beer, R. L., Rovira, M., Huang, W., Wang, G., Gee, S., Vitery Mdel, C., Wheelan, S. J. and Parsons, M. J. (2015). Centroacinar cells are progenitors that contribute to endocrine pancreas regeneration. *Diabetes* **64**, 3499-3509. doi:10.2337/db15-0153

Eames, S. C., Philipson, L. H., Prince, V. E. and Kinkel, M. D. (2010). Blood sugar measurement in zebrafish reveals dynamics of glucose homeostasis. *Zebrafish* **7**, 205-213. doi:10.1089/zeb.2009.0640

Edsbagge, J., Johansson, J. K., Esni, F., Luo, Y., Radice, G. L. and Semb, H. (2005). Vascular function and sphingosine-1-phosphate regulate development of the dorsal pancreatic mesenchyme. *Development* **132**, 1085-1092. doi:10.1242/dev.01643

Field, H. A., Si Dong, P. D., Beis, D. and Stainier, D. Y. R. (2003). Formation of the digestive system in zebrafish. II. Pancreas morphogenesis. *Dev. Biol.* **261**, 197-208. doi:10.1016/S0012-1606(03)00308-7

Freudenblum, J., Iglesias, J. A., Hermann, M., Walsen, T., Wilfinger, A., Meyer, D. and Kimmel, R. A. (2018). In vivo imaging of emerging endocrine cells reveals a requirement for PI3K-regulated motility in pancreatic islet morphogenesis. *Development* **145**, dev158477. doi:10.1242/dev.158477

Gan, W. J., Zavortink, M., Ludick, C., Templin, R., Webb, R., Webb, R., Ma, W., Poronnik, P., Parton, R. G., Gaisano, H. Y. et al. (2017). Cell polarity defines three distinct domains in pancreatic beta-cells. *J. Cell Sci.* **130**, 143-151. doi:10.1242/jcs.185116

Gan, W. J., Do, O. H., Cottle, L., Ma, W., Kosobrodova, E., Cooper-White, J., Bilek, M. and Thorn, P. (2018). Local integrin activation in pancreatic β cells targets insulin secretion to the vasculature. *Cell Rep.* **24**, 2819-2826.e3. doi:10.1016/j.celrep.2018.08.035

Gut, P., Baeza-Raja, B., Andersson, O., Hasenkamp, L., Hsiao, J., Hesselson, D., Akassoglou, K., Verdin, E., Hirschey, M. D. and Stainier, D. Y. R. (2013). Whole-organism screening for gluconeogenesis identifies activators of fasting metabolism. *Nat. Chem. Biol.* **9**, 97-104. doi:10.1038/nchembio.1136

Helker, C. S. M., Mullapudi, S.-T., Mueller, L. M., Preussner, J., Tunaru, S., Skog, O., Kwon, H.-B., Kreuder, F., Lancman, J. J., Bonnavion, R. et al. (2019). Whole organism small molecule screen identifies novel regulators of pancreatic endocrine development. *Development* **146**, dev172569. doi:10.1242/dev.172569

Hen, G., Nicenboim, J., Mayseless, O., Asaf, L., Shin, M., Busolin, G., Hofi, R., Almog, G., Tiso, N., Lawson, N. D. and et al. (2015). Venous-derived angioblasts generate organ-specific vessels during zebrafish embryonic development. *Development* **142**, 4266-4278. doi:10.1242/dev.129247

Hogan, M. F. and Hull, R. L. (2017). The islet endothelial cell: a novel contributor to beta cell secretory dysfunction in diabetes. *Diabetologia* **60**, 952-959. doi:10.1007/s00125-017-4272-9

Hogan, B. M., Bos, F. L., Bussmann, J., Witte, M., Chi, N. C., Duckers, H. J. and Schulte-Merker, S. (2009). Ccbe1 is required for embryonic lymphangiogenesis and venous sprouting. *Nat. Genet.* **41**, 396-398. doi:10.1038/ng.321

Huang, H., Vogel, S. S., Liu, N., Melton, D. A. and Lin, S. (2001). Analysis of pancreatic development in living transgenic zebrafish embryos. *Mol. Cell. Endocrinol.* **177**, 117-124. doi:10.1016/S0303-7207(01)00408-7

Jao, L.-E., Wente, S. R. and Chen, W. (2013). Efficient multiplex biallelic zebrafish genome editing using a CRISPR nuclease system. *Proc. Natl Acad. Sci. USA* **110**, 13904. doi:10.1073/pnas.1308335110

Johansson, M., Mattsson, G., Andersson, A., Jansson, L. and Carlsson, P.-O. (2006). Islet endothelial cells and pancreatic beta-cell proliferation: studies in vitro and during pregnancy in adult rats. *Endocrinology* **147**, 2315-2324. doi:10.1210/en.2005-0997

Jurczyk, A., Roy, N., Bajwa, R., Gut, P., Lipson, K., Yang, C., Covassin, L., Racki, W. J., Rossini, A. A., Phillips, N. et al. (2011). Dynamic glucoregulation and mammalian-like responses to metabolic and developmental disruption in zebrafish. *Gen. Comp. Endocrinol.* **170**, 334-345. doi:10.1016/j.ygcen.2010.10.010

Karra, R., Foglia, M. J., Choi, W.-Y., Belliveau, C., DeBenedittis, P. and Poss, K. D. (2018). Vegfaa instructs cardiac muscle hyperplasia in adult zebrafish. *Proc. Natl Acad. Sci. USA* **115**, 8805. doi:10.1073/pnas.1722594115

Kendall, R. L. and Thomas, K. A. (1993). Inhibition of vascular endothelial cell growth factor activity by an endogenously encoded soluble receptor. *Proc. Natl. Acad. Sci. USA* **90**, 10705-10709. doi:10.1073/pnas.90.22.10705

Koch, S. and Claesson-Welsh, L. (2012). Signal transduction by vascular endothelial growth factor receptors. *Cold Spring Harb. Perspect. Med.* **2**, a006502. doi:10.1101/cshperspect.a006502

Lammert, E., Cleaver, O. and Melton, D. (2001). Induction of pancreatic differentiation by signals from blood vessels. *Science* **294**, 564-567. doi:10.1126/science.1064344

Lawson, N. D. and Weinstein, B. M. (2002). In vivo imaging of embryonic vascular development using transgenic zebrafish. *Dev. Biol.* **248**, 307-318. doi:10.1006/dbio.2002.0711

Lifson, N., Lassa, C. V. and Dixit, P. K. (1985). Relation between blood flow and morphology in islet organ of rat pancreas. *Am. J. Physiol.* **249**, E43-E48. doi:10.1152/ajpendo.1985.249.1.E43

Lu, J., Liu, K. C., Schulz, N., Karampelias, C., Charbord, J., Hilding, A., Rautio, L., Bertolino, P., Östenson, C. G., Brismar, K. et al. (2016). IGFBP1 increases beta-cell regeneration by promoting alpha- to beta-cell transdifferentiation. *EMBO J.* **35**, 2026-2044. doi:10.15252/embj.201592903

Magenheim, J., Ilovich, O., Lazarus, A., Klochendler, A., Ziv, O., Werman, R., Hija, A., Cleaver, O., Mishani, E., Keshet, E. et al. (2011). Blood vessels restrain pancreas branching, differentiation and growth. *Development* **138**, 4743. doi:10.1242/dev.066548

Manfroid, I., Ghaye, A., Naye, F., Detry, N., Palm, S., Pan, L., Ma, T. P., Huang, W., Rovira, M., Martial, J. A. et al. (2012). Zebrafish sox9b is crucial for hepatopancreatic duct development and pancreatic endocrine cell regeneration. *Dev. Biol.* **366**, 268-278. doi:10.1016/j.ydbio.2012.04.002

Matsuda, H., Parsons, M. J. and Leach, S. D. (2013). Aldh1-expressing endocrine progenitor cells regulate secondary islet formation in larval zebrafish pancreas. *PLoS ONE* **8**, e74350. doi:10.1371/journal.pone.0074350

Matsuda, H., Mullapudi, S. T., Yang, Y. H. C., Masaki, H., Hesselson, D. and Stainier, D. Y. R. (2018). Whole-organism chemical screening identifies modulators of pancreatic beta-cell function. *Diabetes* **67**, 2268-2279. doi:10.2337/db17-1223

Matsuoka, R. L., Marass, M., Avdesh, A., Helker, C. S. M., Maischein, H.-M., Grosse, A. S., Kaur, H., Lawson, N. D., Herzog, W. and Stainier, D. Y. R. (2016). Radial glia regulate vascular patterning around the developing spinal cord. *eLife* **5**, e20253. doi:10.7554/eLife.20253

Mattsson, G., Jansson, L. and Carlsson, P.-O. (2002). Decreased vascular density in mouse pancreatic islets after transplantation. *Diabetes* **51**, 1362-1366. doi:10.2337/diabetes.51.5.1362

Mitola, S., Ravelli, C., Moroni, E., Salvi, V., Leali, D., Ballmer-Hofer, K., Zammataro, L. and Presta, M. (2010). Gremlin is a novel agonist of the major proangiogenic receptor VEGFR2. *Blood* **116**, 3677-3680. doi:10.1182/blood-2010-06-291930

Mullapudi, S. T., Helker, C. S. M., Boezio, G. L. M., Maischein, H.-M., Sokol, A. M., Guenther, S., Matsuda, H., Kubicek, S., Graumann, J., Yang, Y. H. C. et al. (2018). Screening for insulin-independent pathways that modulate glucose homeostasis identifies androgen receptor antagonists. *eLife* **7**, e42209. doi:10.7554/eLife.42209

Nikolova, G., Strilic, B. and Lammert, E. (2007). The vascular niche and its basement membrane. *Trends Cell Biol.* **17**, 19-25. doi:10.1016/j.tcb.2006.11.005

Nikolova, G., Jabs, N., Konstantinova, I., Domogatskaya, A., Tryggvason, K., Sorokin, L., Fässler, R., Gu, G., Gerber, H.-P., Ferrara, N. et al. (2006). The vascular basement membrane: a niche for insulin gene expression and Beta cell proliferation. *Dev. Cell* **10**, 397-405. doi:10.1016/j.devcel.2006.01.015

Ninov, N., Borius, M. and Stainier, D. Y. R. (2012). Different levels of Notch signaling regulate quiescence, renewal and differentiation in pancreatic endocrine progenitors. *Development* **139**, 1557-1567. doi:10.1242/dev.076000

Ober, E. A., Field, H. A. and Stainier, D. Y. R. (2003). From endoderm formation to liver and pancreas development in zebrafish. *Mech. Dev.* **120**, 5-18. doi:10.1016/S0925-4773(02)00327-1

Obholzer, N., Wolfson, S., Trapani, J. G., Mo, W., Nechiporuk, A., Busch-Nentwich, E., Seiler, C., Sidi, S., Sollner, C., Duncan, R. N. et al. (2008). Vesicular glutamate transporter 3 is required for synaptic transmission in zebrafish hair cells. *J. Neurosci.* **28**, 2110-2118. doi:10.1523/JNEUROSCI.5230-07.2008

Parnaud, G., Hammar, E., Ribaux, P., Donath, M. Y., Berney, T. and Halban, P. A. (2009). Signaling pathways implicated in the stimulation of beta-cell proliferation by extracellular matrix. *Mol. Endocrinol.* **23**, 1264-1271. doi:10.1210/me.2009-0008

Peiris, H., Bonder, C. S., Coates, P. T., Keating, D. J. and Jessup, C. F. (2014). The beta-cell/EC axis: how do islet cells talk to each other? *Diabetes* **63**, 3-11. doi:10.2337/db13-0617

Pepper, A. R., Gala-Lopez, B., Ziff, O. and Shapiro, A. M. J. (2013). Revascularization of transplanted pancreatic islets and role of the transplantation site. *Clin. Dev. Immunol.* **2013**, 352315. doi:10.1155/2013/352315

Ravier, M. A., Guldenagel, M., Charollais, A., Gjinovci, A., Caille, D., Sohl, G., Wollheim, C. B., Willecke, K., Henquin, J.-C. and Meda, P. (2005). Loss of connexin36 channels alters beta-cell coupling, islet synchronization of glucose-induced $Ca2^+$ and insulin oscillations, and basal insulin release. *Diabetes* **54**, 1798-1807. doi:10.2337/diabetes.54.6.1798

Reinert, R. B., Brissova, M., Shostak, A., Pan, F. C., Poffenberger, G., Cai, Q., Hundemer, G. L., Kantz, J., Thompson, C. S., Dai, C. et al. (2013). Vascular endothelial growth factor-a and islet vascularization are necessary in developing, but not adult, pancreatic islets. *Diabetes* **62**, 4154-4164. doi:10.2337/db13-0071

Rossi, A., Gauvrit, S., Marass, M., Pan, L., Moens, C. B. and Stainier, D. Y. R. (2016). Regulation of Vegf signaling by natural and synthetic ligands. *Blood* **128**, 2359-2366. doi:10.1182/blood-2016-04-711192

Salem, V., Silva, L. D., Suba, K., Georgiadou, E., Gharavy, S. N. M., Akhtar, N., Martin-Alonso, A., Gaboriau, D. C. A., Rothery, S. M., Stylianides, T. et al. (2019). Leader β-cells coordinate Ca2+ dynamics across pancreatic islets in vivo. *Nat. Metab.* **1**, 615-629. doi:10.1038/s42255-019-0075-2

Shalaby, F., Rossant, J., Yamaguchi, T. P., Gertsenstein, M., Wu, X.-F., Breitman, M. L. and Schuh, A. C. (1995). Failure of blood-island formation and vasculogenesis in Flk-1-deficient mice. *Nature* **376**, 62-66. doi:10.1038/376062a0

Steiner, D. J., Kim, A., Miller, K. and Hara, M. (2010). Pancreatic islet plasticity: interspecies comparison of islet architecture and composition. *Islets* **2**, 135-145. doi:10.4161/isl.2.3.11815

Tarifeño-Saldivia, E., Lavergne, A., Bernard, A., Padamata, K., Bergemann, D., Voz, M. L., Manfroid, I. and Peers, B. (2017). Transcriptome analysis of pancreatic cells across distant species highlights novel important regulator genes. *BMC Biol.* **15**, 21. doi:10.1186/s12915-017-0362-x

Thermes, V., Grabher, C., Ristoratore, F., Bourrat, F., Choulika, A., Wittbrodt, J. and Joly, J.-S. (2002). I-SceI meganuclease mediates highly efficient transgenesis in fish. *Mech. Dev.* **118**, 91-98. doi:10.1016/S0925-4773(02)00218-6

Toselli, C. M., Wilkinson, B. M., Paterson, J. and Kieffer, T. J. (2019). Vegfa/vegfr2 signaling is necessary for zebrafish islet vessel development, but is dispensable for beta-cell and alpha-cell formation. *Sci. Rep.* **9**, 3594. doi:10.1038/s41598-019-40136-1

Traver, D., Paw, B. H., Poss, K. D., Penberthy, W. T., Lin, S. and Zon, L. I. (2003). Transplantation and in vivo imaging of multilineage engraftment in zebrafish bloodless mutants. *Nat. Immunol.* **4**, 1238-1246. doi:10.1038/ni1007

Varshney, G. K., Pei, W., LaFave, M. C., Idol, J., Xu, L., Gallardo, V., Carrington, B., Bishop, K., Jones, M. P., Li, M. et al. (2015). High-throughput gene targeting and phenotyping in zebrafish using CRISPR/Cas9. *Genome Res.* **25**, 1030-1042. doi:10.1101/gr.186379.114

Villasenor, A. and Stainier, D. Y. R. (2017). On the development of the hepatopancreatic ductal system. *Semin Cell Dev Biol.* **66**, 69-80. doi:10.1016/j.semcdb.2017.02.003

Yang, Y. H. C., Kawakami, K. and Stainier, D. Y. R. (2018). A new mode of pancreatic islet innervation revealed by live imaging in zebrafish. *eLife* **7**, e34519. doi:10.7554/eLife.34519

Ye, L., Robertson, M. A., Hesselson, D., Stainier, D. Y. R. and Anderson, R. M. (2015). Glucagon is essential for alpha cell transdifferentiation and beta cell neogenesis. *Development* **142**, 1407-1417. doi:10.1242/dev.117911

Yoshitomi, H. and Zaret, K. S. (2004). Endothelial cell interactions initiate dorsal pancreas development by selectively inducing the transcription factor Ptf1a. *Development* **131**, 807. doi:10.1242/dev.00960

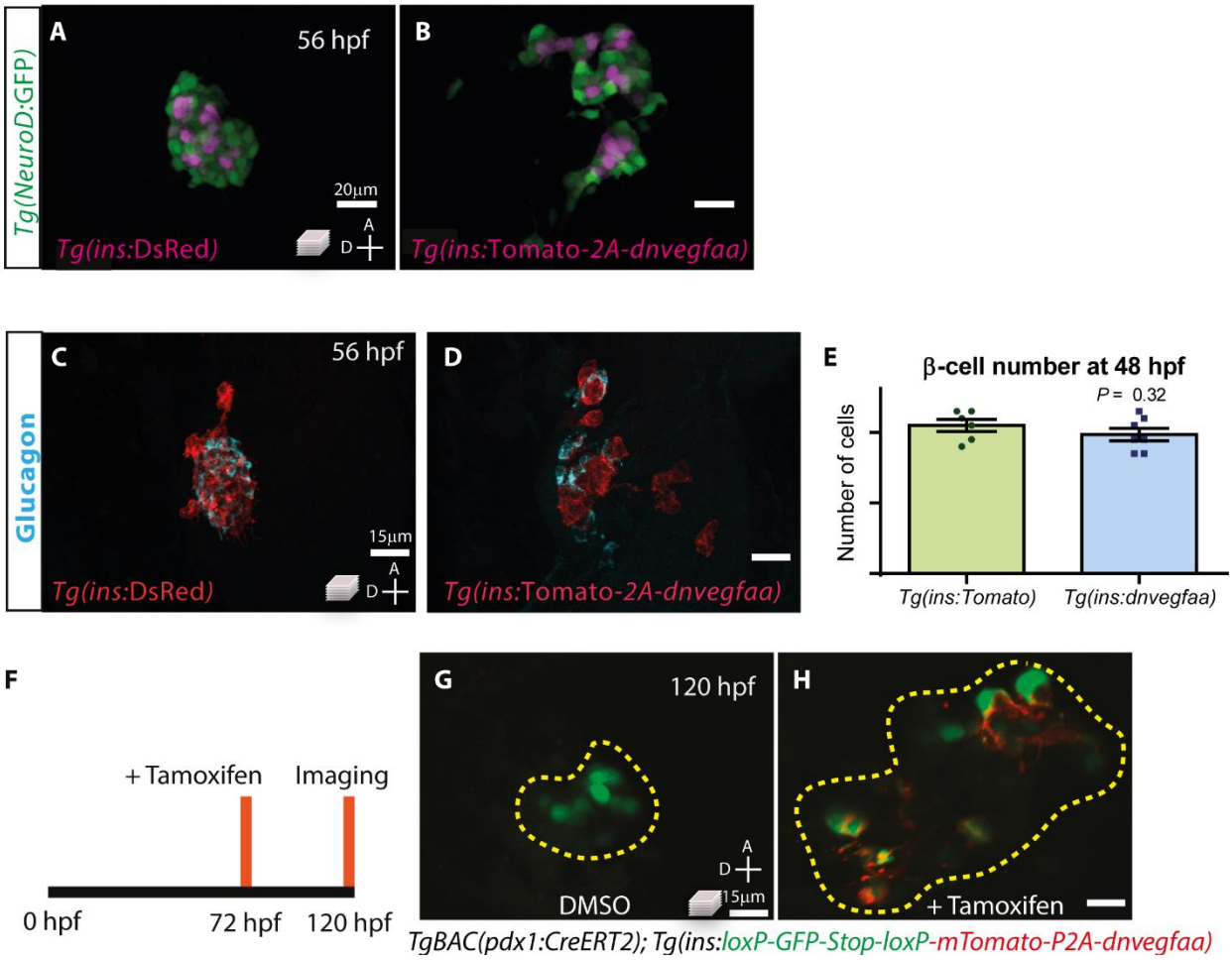

Figure S1: β-cell specific expression of dnVegfaa at embryonic or post-embryonic stages results in islet disruption. A-B) Pancreatic endocrine cells (green) in 56 hpf *Tg(NeuroD:GFP); Tg(ins:DsRed)* and *Tg(NeuroD:GFP); Tg(ins:dnvegfaa)* embryos. C-D) Confocal projection images of the pancreatic islet in 56 hpf *Tg(ins:DsRed)* and *Tg(ins:dnvegfaa)* animals showing Glucagon-positive α-cells (cyan). E) Number of β-cells in 48 hpf *Tg(ins:dnvegfaa)* and *Tg(ins:DsRed)* animals; mean ± SEM, n = 6-7 animals. *P* values from t-tests are presented. F) Induction of *dnVegfaa* expression in *TgBAC(pdx1:CreERT2); Tg(ins:loxP-GFP-STOP-loxP-mTom-P2A-dnVegfaa)* animals with 10 µM Tamoxifen treatment starting at 72 hpf and imaging at 120 hpf. G-H) β-cells in 120 hpf *TgBAC(pdx1:CreERT2); Tg(ins:loxP-GFP-STOP-loxP-mTom-P2A-dnvegfaa)* larvae treated with DMSO (vehicle) or Tamoxifen. Yellow dotted lines outline the spread of the β-cells in the primary islet. Maximum intensity projections are presented; A, anterior; D, dorsal.

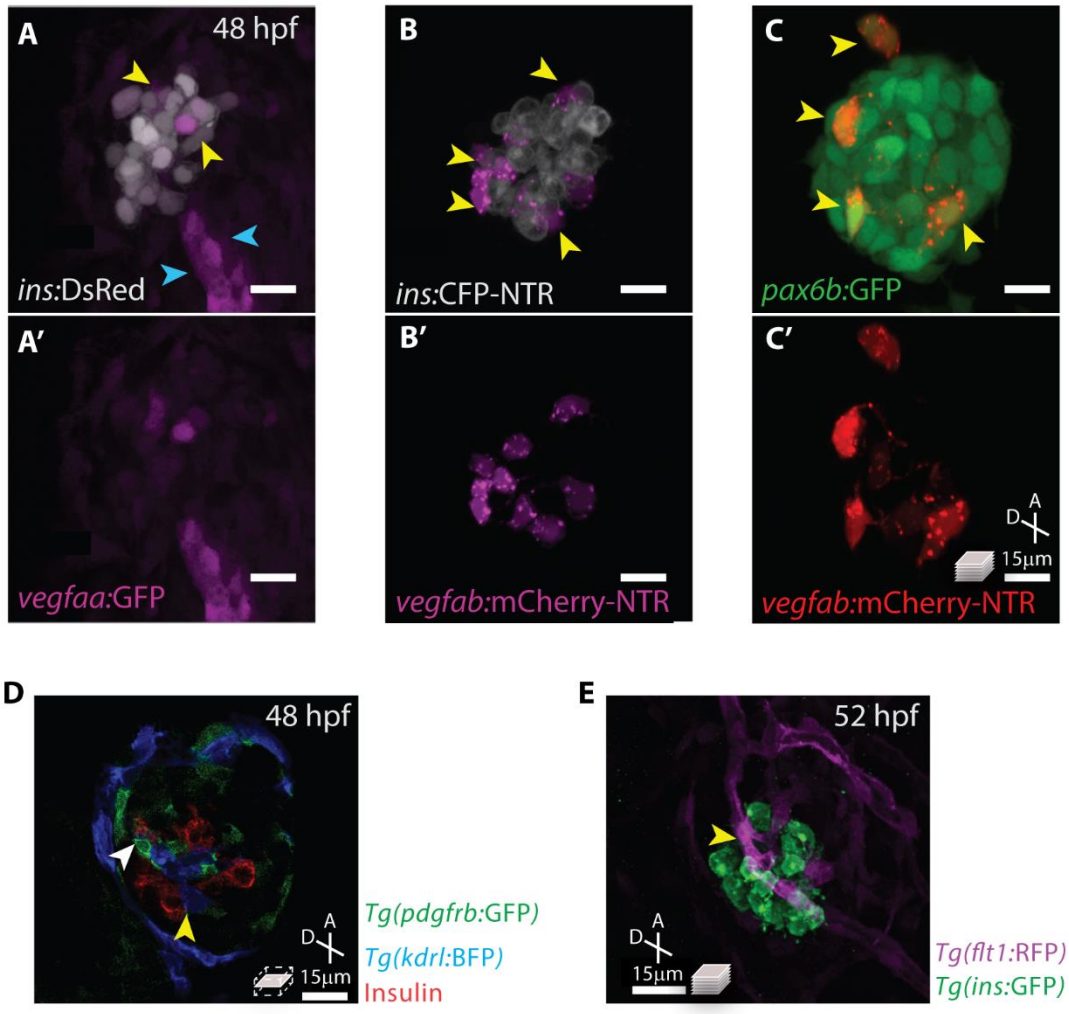

Figure S2: *vegfaa* and *vegfab* are expressed in and around the pancreatic endocrine cells. A) β-cells (white) in 48 hpf *TgBAC(vegfaa:GFP); Tg(ins:DsRed)* embryos. Yellow arrowheads point to *vegfaa* expressing β-cells. Blue arrowheads point to *vegfaa* expressing cells close to the islet that likely belong to non-endocrine lineages. B) β-cells (white) in 48 hpf *TgBAC(vegfab:gal4ff); Tg(UAS-E1b:Nfsb-mCherry); Tg(ins:CFP-NTR)* embryos. *TgBAC(vegfab:gal4ff);Tg(UAS-E1b:NfsB-mCherry)* is referred to as *Tg(vegfab:mCherry-NTR)*. Yellow arrowheads point to *vegfab* expressing cells around β-cells. C) Pancreatic endocrine cells (green) in 48 hpf *Tg(vegfab:mCherryNTR); Tg(pax6b:GFP)* embryos. Yellow arrowheads point to *vegfab* expressing endocrine cells. Maximum intensity projections are presented. D) Confocal plane of the primary pancreatic islet in a 48 hpf *Tg(kdrl:BFP); Tg(pdgfrb:GFP)* embryo showing β-cells (red). Yellow arrowhead points to a *kdrl* expressing endothelial cell in contact with a β-cell. White arrowhead points to a *pdgfrb* expressing cell in contact with a β-cell. E) Confocal projection image of the primary pancreatic islet in a 52 hpf *Tg(ins:GFP); Tg(flt1:RFP)* embryo showing β-cells (green). Yellow arrowhead points to a *flt1* expressing blood vessel in the islet. ; A, anterior; D, dorsal.

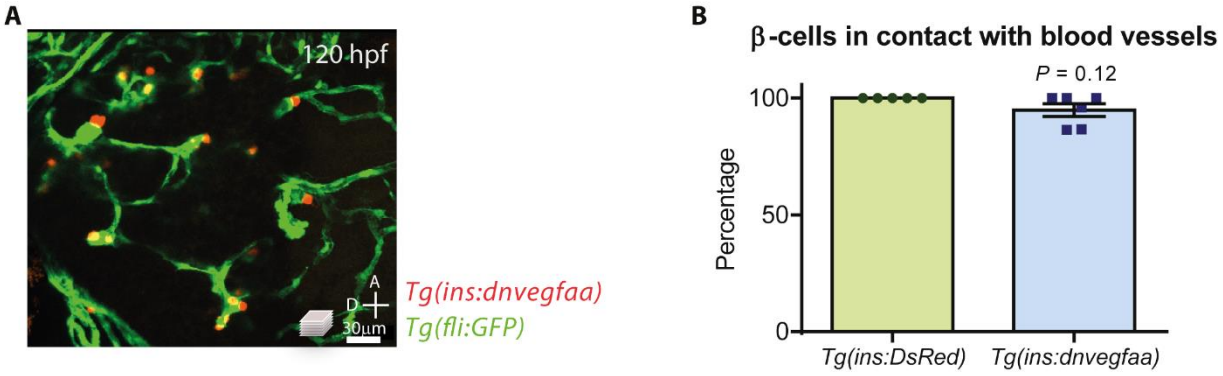

Figure S3: β-cells in *Tg(ins:dnvegfaa)* animals are in contact with blood vessels. A) Confocal projection image of the pancreatic islet in a 120 hpf *Tg(ins:dnvegfaa);Tg(fli:GFP)* animal showing β-cells (red). Maximum intensity projection is presented. B) Percentage of β-cells in contact with blood vessels in 120 hpf *Tg(ins:DsRed)* and *Tg(ins:dnvegfaa)* animals; mean ± SEM, n = 6-7 animals. *P* values from t-tests are presented.

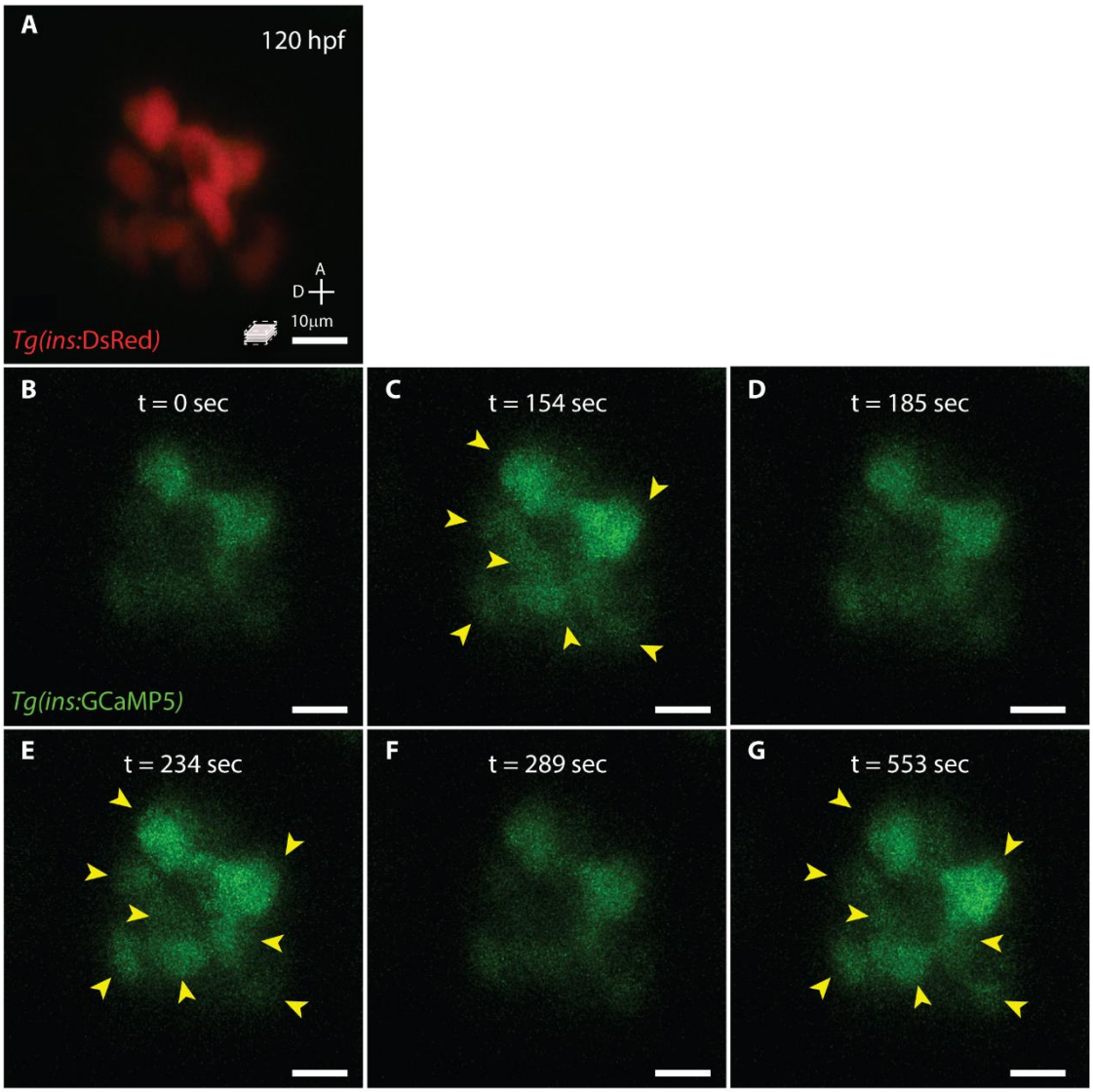
A
120 hpf
A
D
10μm
Tg(ins:DsRed)
B
t = 0 sec
C
t = 154 sec
D
t = 185 sec
Tg(ins:GCaMP5)
E
t = 234 sec
F
t = 289 sec
G
t = 553 sec

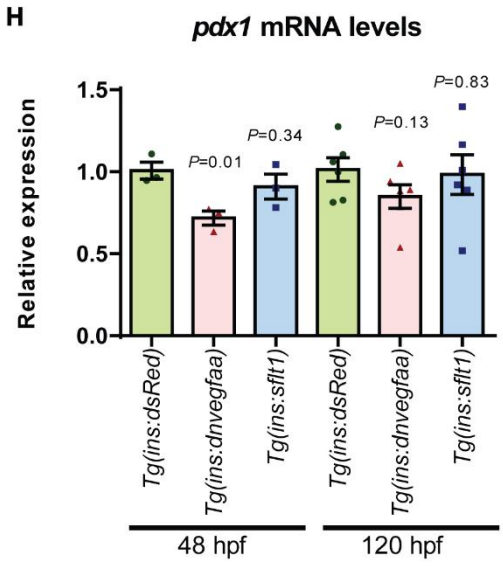
H
pdx1 mRNA levels
Relative expression
1.5
1.0
0.5
0.0
P=0.01
P=0.34
P=0.13
P=0.83
Tg(ins:dsRed)
Tg(ins:dnvegfaa)
Tg(ins:sflt1)
Tg(ins:dsRed)
Tg(ins:dnvegfaa)
Tg(ins:sflt1)
48 hpf
120 hpf

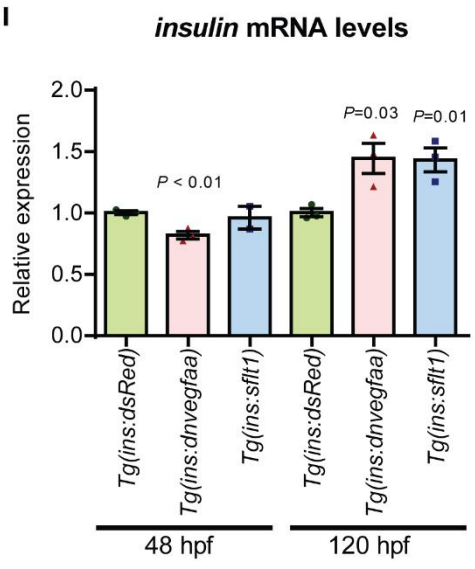
I
insulin mRNA levels
Relative expression
2.0
1.5
1.0
0.5
0.0
P < 0.01
P=0.03
P=0.01
Tg(ins:dsRed)
Tg(ins:dnvegfaa)
Tg(ins:sflt1)
Tg(ins:dsRed)
Tg(ins:dnvegfaa)
Tg(ins:sflt1)
48 hpf
120 hpf

Figure S4: Live imaging shows dynamics of calcium signaling in β-cells. A) Pancreatic β-cells (red) in 120 hpf *Tg(ins:DsRed); Tg(ins:GCaMP5)* animals. B-G) Calcium responsive fluorescence signal in 120 hpf *Tg(ins:DsRed); Tg(ins:GCaMP5)* animals, at the indicated time point, from live confocal imaging. Yellow arrowheads point to β-cells showing an observable increase in fluorescence signal intensity. Maximum intensity projections of planes in the central 30 μm region of the islet are shown. A, anterior; D, dorsal. H-I) *pdx1* (H) and *ins* (I) mRNA levels in 48 and 120 hpf animals; 3-6 replicates, 10 animals per replicate, mean ± SEM. *P* values from t-tests are presented.

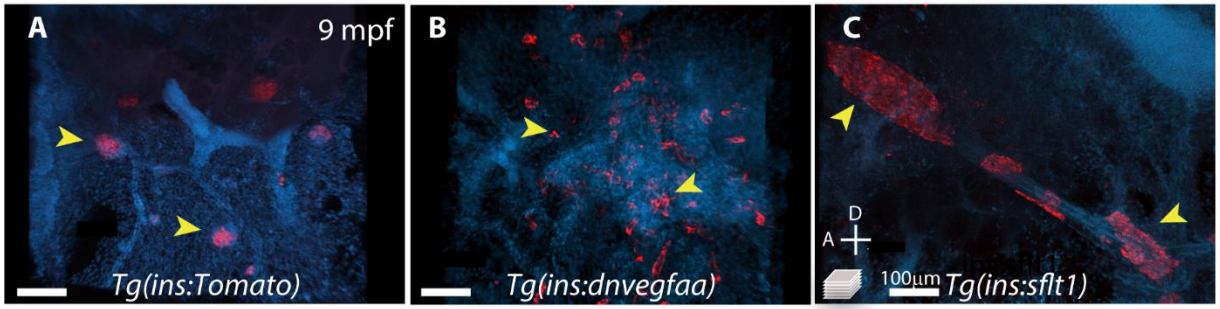

Insulin DNA

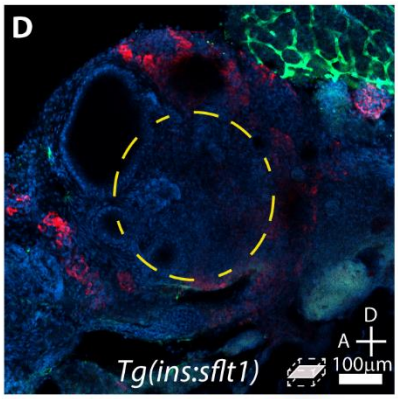

Insulin *Tg(fli:*GFP) DNA

E

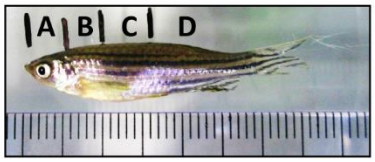

F

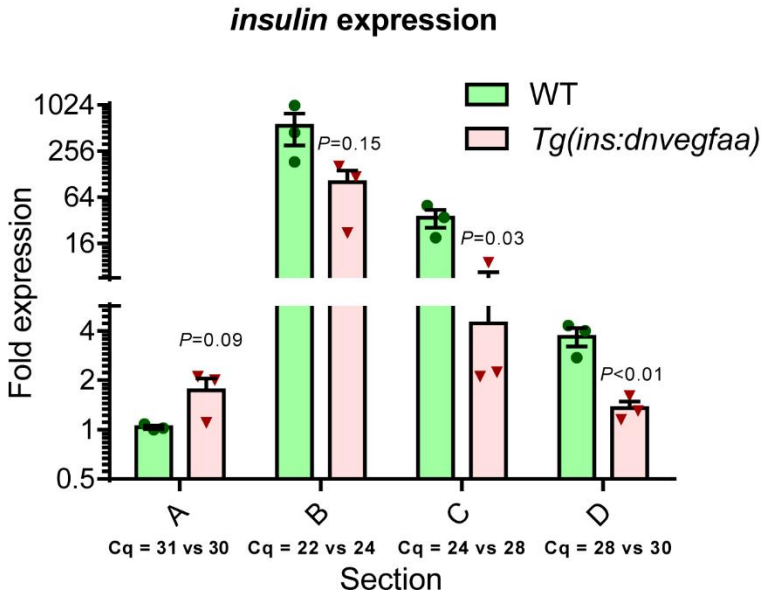

G

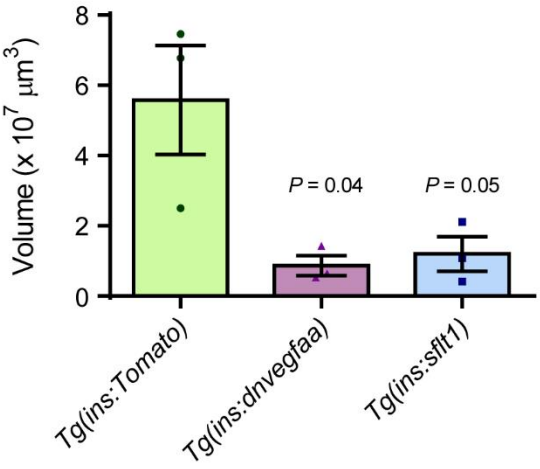

H

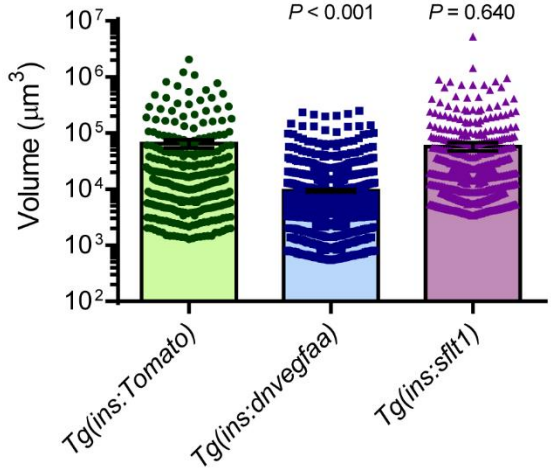

Figure S5: β-cell specific expression of dnVegfaa or sFlt1 causes defects in secondary islet formation. A-C) Wholemount immunostaining for β-cells (Insulin) along the pancreatic ducts of 9 mpf zebrafish after CLARITY-based tissue clearing. Yellow arrowheads point to β-cell clusters. D) Wholemount immunostaining for β-cells (Insulin) in the primary islet of a 9 mpf *Tg(ins:sflt1); Tg(fli:GFP)* zebrafish after CLARITY-based tissue clearing. Yellow dotted line outlines the nuclei in the core of the islet. E) Adult zebrafish divided up into four sections, as marked, to obtain RNA and quantify *insulin* expression in each section separately; section A - head, heart, eyes; section B - anterior gastrointestinal (GI) tract; section C - posterior GI tract; section D - lower trunk and tail regions. F) *insulin* mRNA levels (qPCR) from each of the four sections along with Ct values. G) Volume of Insulin antibody immunostaining (β-cells) in adult zebrafish pancreas, computed using surface construction in Imaris. H) Volume of Insulin antibody immunostaining (β-cells) in secondary islets, computed using surface construction in Imaris. Data points greater than 5.0×10^5 μm^3 in *Tg(ins:Tomato)* and *Tg(ins:sflt1)* animals correspond to the largest secondary islet clusters located close to the primary islet (Figure 4), mean ± SEM, n = 3 animals, 100 to 560 secondary islets per animal, *P* values from t-tests are presented.

	Ensembl Gene ID	Gene	Normalized Read Count (β-cells)	% of pancreatic cells with expression
Ligands	ENSDARG00000035350	*ins*	4324351	99.76
	ENSDARG00000103542	*vegfaa*	4101	6.64
	ENSDARG00000034700	*vegfab*	11588	13.72
	ENSDARG00000069640	*vegfc*	0	0.4
	ENSDARG00000092480	*vegfbb*	0	ND
	ENSDARG00000077588	*pdgfc*	147	0.56
	ENSDARG00000058424	*pdgfab*	420	1.61
	ENSDARG00000055505	*pdgfaa*	194	1.05
	ENSDARG00000077677	*pdgfd*	442	ND
	ENSDARG00000038139	*pdgfbb*	0	0.93
	ENSDARG00000005001	*grem2*	178	1.57
Receptors	ENSDARG00000019371	*flt1*	1	1.01
	ENSDARG00000017321	*kdr*	0	0.08
	ENSDARG00000105215	*kdrl*	16	1.97
	ENSDARG00000015717	*flt4*	1	0.64
	ENSDARG00000070494	*pdgfra*	2	0.68
	ENSDARG00000100897	*pdgfrb*	0	ND
	ENSDARG00000006456	*pdgfrl*	755	0.60
	ENSDARG00000027290	*nrp1b*	58	0.32
	ENSDARG00000071865	*nrp1a*	139	2.01
	ENSDARG00000096546	*nrp2a*	175	0.40
	ENSDARG00000038446	*nrp2b*	0	0.20

Table S1: Pancreatic β-cell expression of Vegf family ligand and receptor genes. Normalized read counts (Tarifeño-Saldivia et al., 2017) and percentage of pancreatic cells (Salem et al., 2019) expressing different Vegf family ligand and receptor genes; ND, not detected.

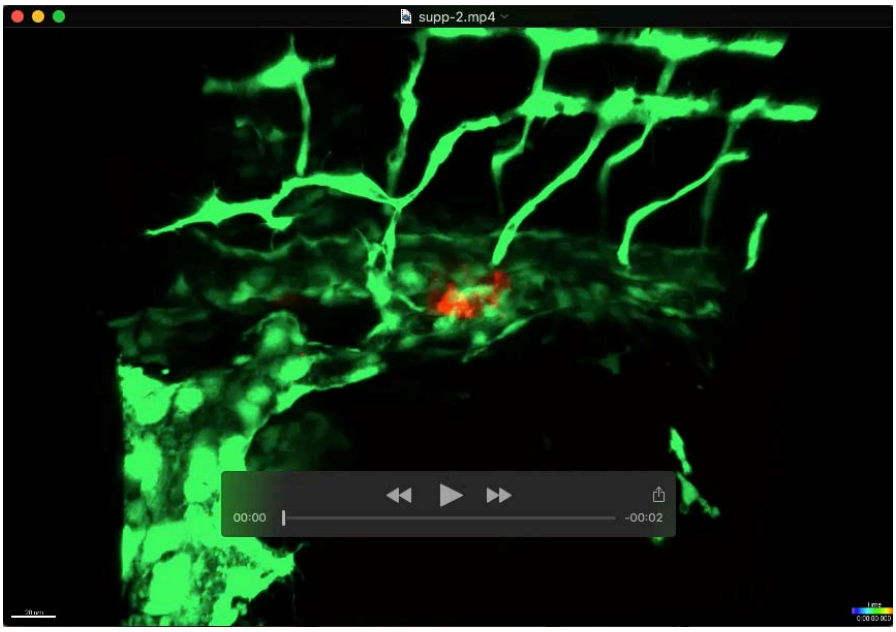

Movie 1: Time-lapse imaging shows collective migration of β-cells and their interaction with the vasculature in wild-type embryos. Confocal imaging of *Tg(ins:Tomato); Tg(fli:GFP)* zebrafish from 34 to 48 hpf at 60 min time intervals. Movie corresponds to Figure 1e.

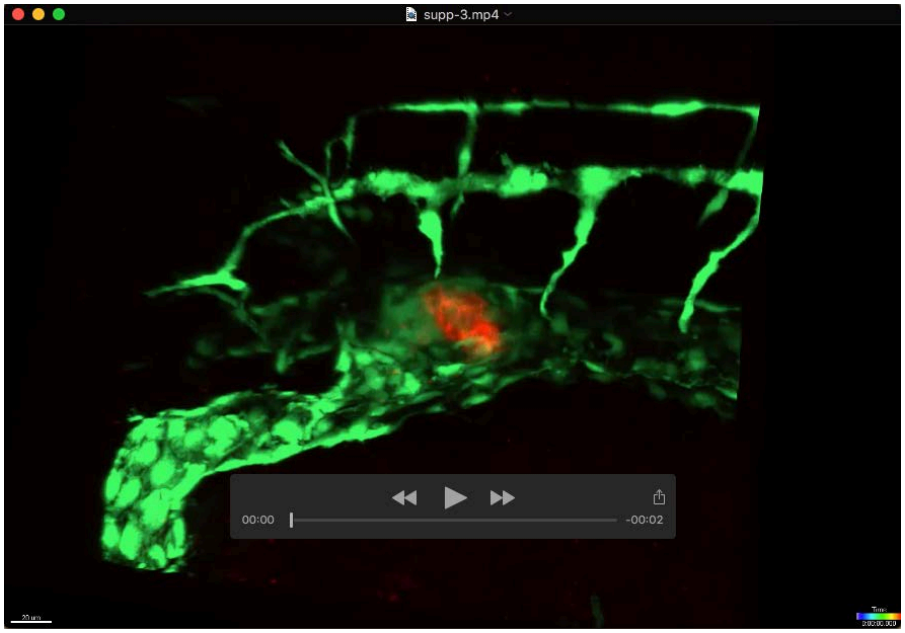

Movie 2: Time-lapse imaging shows dispersion of β-cells in *Tg(ins:dnvegfaa)* embryos. Confocal imaging of *Tg(ins:dnvegfaa); Tg(fli:GFP)* zebrafish from 34 to 48 hpf at 60 min time intervals. β-cells are marked in red. Movie corresponds to Figure 1f.

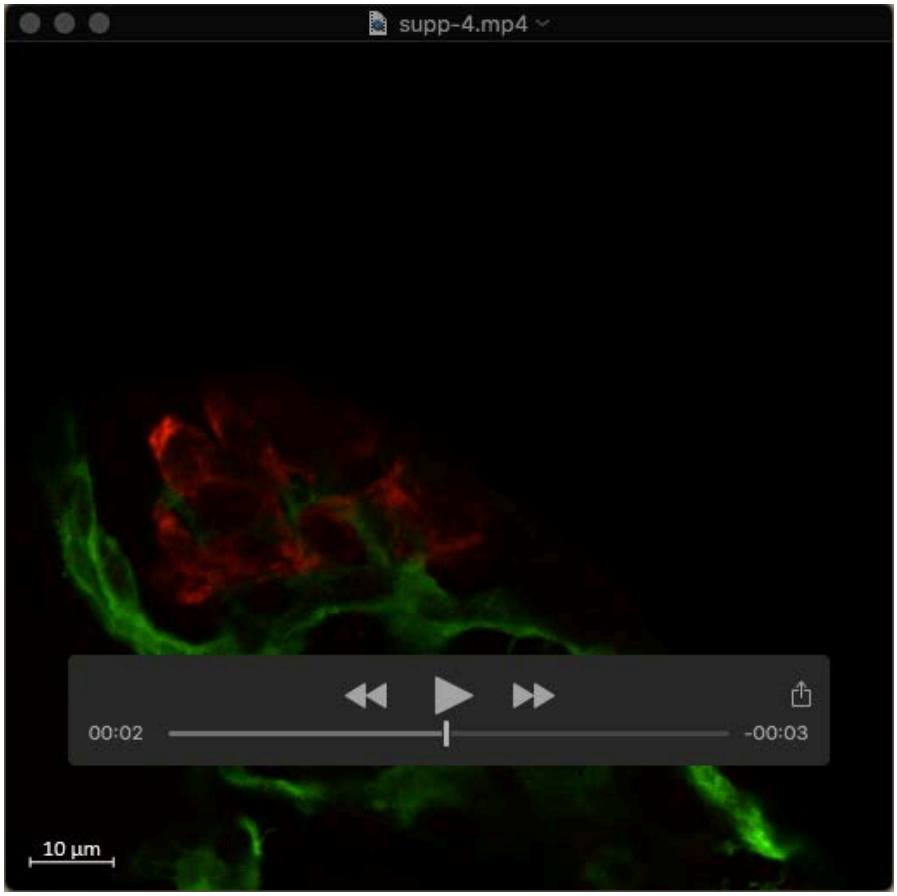

Movie 3: Wild-type pancreatic islets contain intra-islet vessels. Progressive planes in a Z-stack from confocal imaging of pancreatic islets in 48 hpf *Tg(ins:DsRed); Tg(fli:GFP)* zebrafish, with immunostaining for Insulin (red) and GFP. Movie corresponds to Figure 2c.

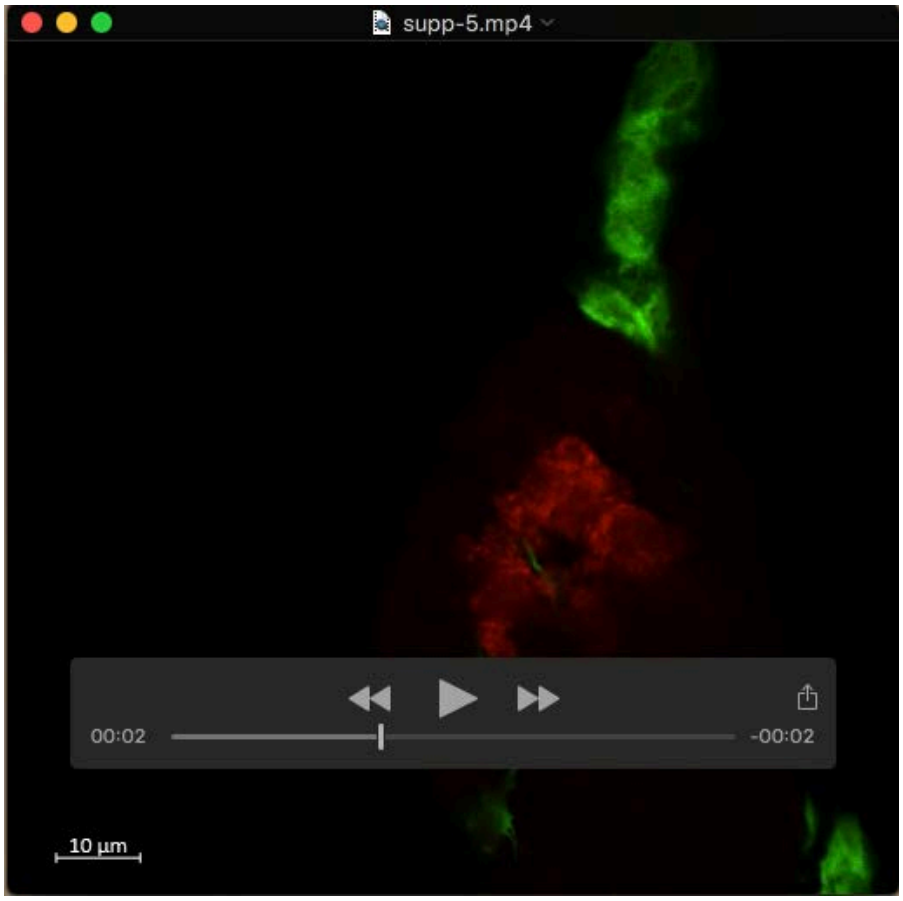

Movie 4: β-cell-specific sFlt1 expression results in markedly reduced intra-islet vasculature.
Progressive planes in a Z-stack from confocal imaging of pancreatic islets in 48 hpf *Tg(ins:sflt1); Tg(fli:GFP)* zebrafish, after immunostaining for Insulin (red) and GFP. Movie corresponds to Figure 2j.

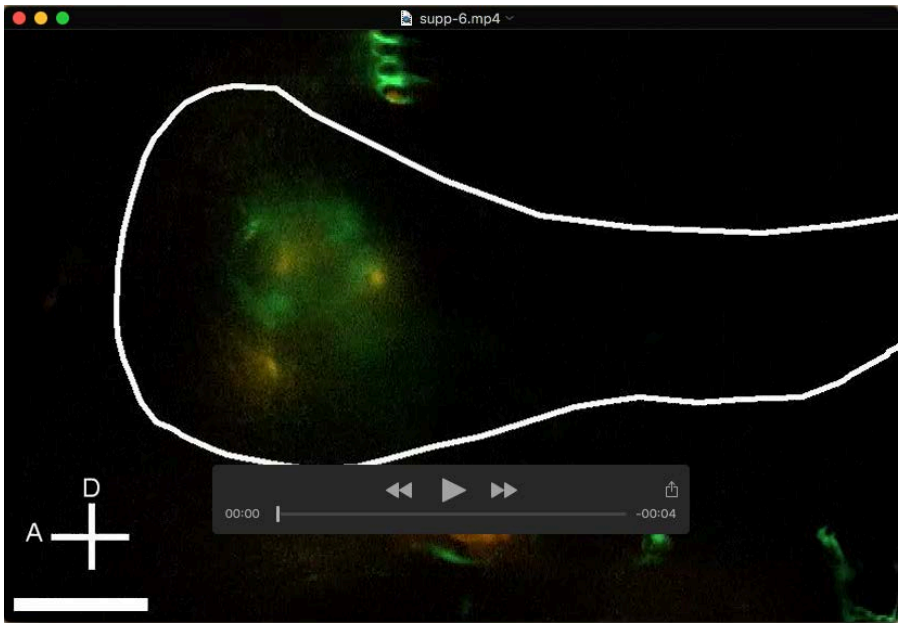

Movie 5: Live imaging shows circulating red blood cells in wild-type larval pancreas. Spinning disk confocal imaging of the pancreatic islet in 120 hpf *Tg(gata1:DsRed); Tg(fli:GFP)* zebrafish, showing circulating red blood cells (red). Pancreas is outlined in white. Scale bar, 40 μm.

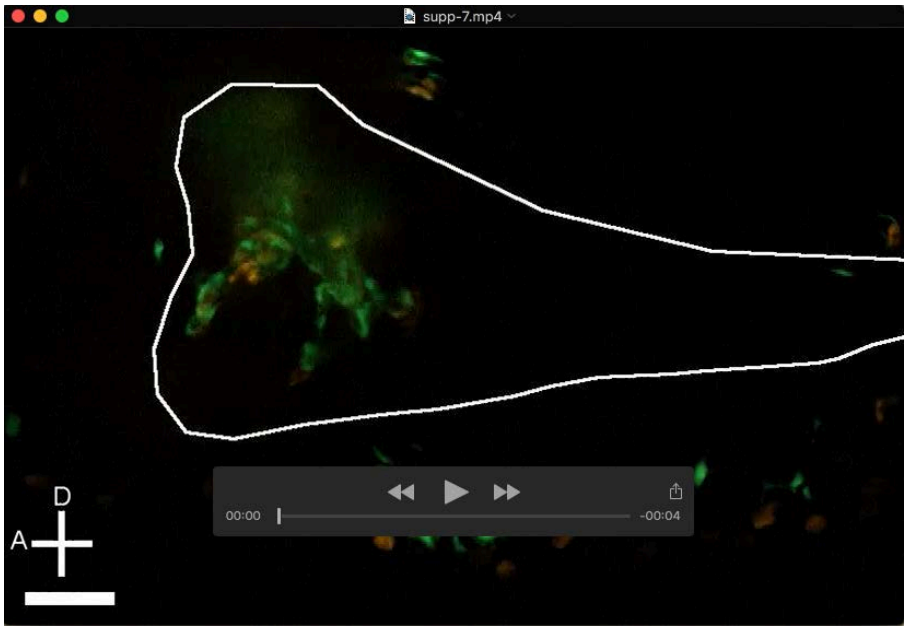

Movie 6: Live imaging shows circulating red blood cells and disrupted vasculature in *Tg(ins:dnvegfaa)* pancreas. Spinning disk confocal imaging of the pancreatic islet in 120 hpf *Tg(ins:dnvegfaa); Tg(gata1:DsRed); Tg(fli:GFP)* zebrafish. Pancreas is outlined in white. Scale bar, 40 μm.

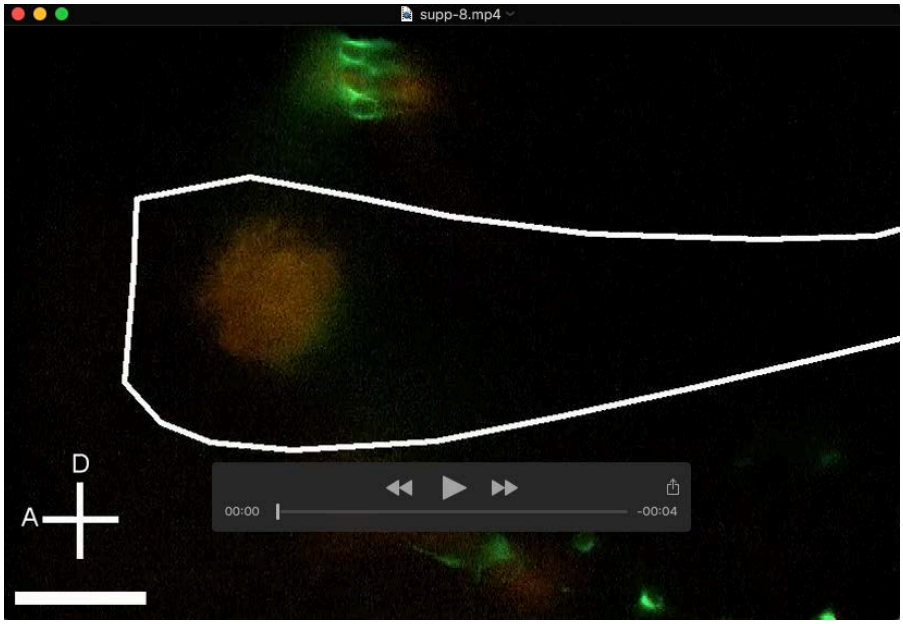

Movie 7: Live imaging shows lack of vasculature and circulation in *Tg(ins:sflt1)* pancreas. Spinning disk confocal imaging of the pancreatic islet in 120 hpf *Tg(ins:sflt1); Tg(gata1:DsRed); Tg(fli:GFP)* zebrafish. Faint red signal in the anterior region of the pancreas (outlined in white) is from β-cells. Scale bar, 40 μm.

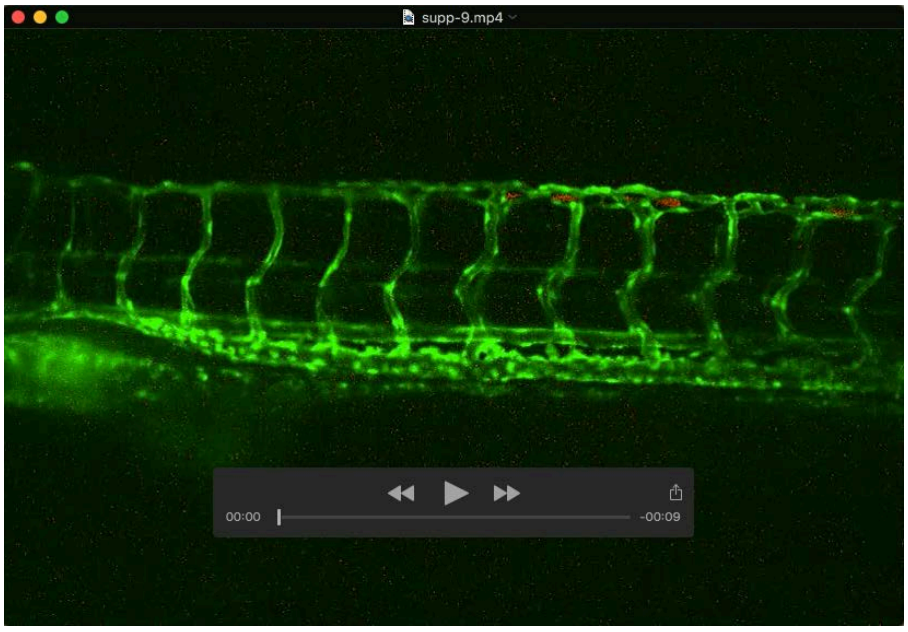

Movie 8: Live imaging shows circulating β-cell in *Tg(ins:dnvegfaa)* larvae. Spinning disk confocal imaging of 72 hpf *Tg(ins:dnvegfaa); Tg(fli:GFP)* zebrafish. Arrowhead points to the β-cells circulating in the trunk region.